2003

RCK Domain Model of Calcium Activation in BK Channels

Alexander R. Pico

RCK Domain Model of Calcium Activation in BK Channels

A thesis presented to the faculty of
The Rockefeller University
in partial fulfillment of the requirements for
the degree of Doctor of Philosophy

by

Alexander R. Pico

TO MY FATHER, RICHARD MICHAEL PICO,

FOR SHOWING ME THE LIGHT OF SCIENCE IN THIS DEMON-HAUNTED WORLD.

falling rock through space
bleak if not so imagined
as a wondrous place

ACKNOWLEDGEMENT

I have worked with a true, sweat-and-blood genius, Dr. Roderick MacKinnon, along with a laboratory of the most intellectually talented, driven, and sincere group of people one should ever hope to work with, and I am truly grateful. I am particularly indebted to the collaboration with Dr. Youxing Jiang for work that gave form to my project.

I would like to thank my faculty advisory committee for their time and attention and for their comments and corrections: Dr. David Gadsby, Dr. Andrej Šali, and Dr. Eric Gouaux. I would especially like to thank Dr. John Kuriyan for mentoring my first endeavor at The Rockefeller University as a summer undergraduate student, providing my first introduction to the methods of modern biology.

And a thank you to the hard working secretaries of The Dean's Office. Marta Delgado and Kristen Cullen deserve special acknowledgement for their loyalty and commitment to the graduate students.

TABLE OF CONTENTS

TABLE OF FIGURES

ABSTRACT

Potassium ion channels are ubiquitously expressed from bacteria to mammals where they are involved in various processes ranging from the regulation of osmotic pressure in a single cell to the electrical response in muscle fibers to the generation of action potentials in neurons. The BK channel family (BK for Big K^+ conductance) is an interesting subfamily of K^+ channels responsive to both membrane voltage and intracellular calcium ion. The unique, high-affinity Ca^{2+} sensitivity of BK channels is critical to their physiological function in various cell types. The mechanism by which Ca^{2+} activates BK channel gating, however, is not well understood. Here we present a structure-based approach to the study of BK channels with the goal of providing a structural and functional model of the Ca^{2+}-activation mechanism. Sequence analysis of BK channel C-terminal domains and domains from prokaryotic homologs reveals the conservation of unique positions defining a novel regulatory domain associated with K^+ conduction, the RCK domain. Crystal structures of RCK domains from prokaryotic sources relate the conservation of sequence to the structure, assembly and function of these domains. We propose a hypothetical model for the structure and function of the C-terminal domains of BK as a set of RCK domains that conduct the Ca^{2+}-activation mechanism. The features and constraints predicted by the RCK domain model are tested by the electrophysiological assay of a variety of human BK constructs. The results support a domain structure and assembly consistent with the proposed model for the BK C-terminus. In addition, the results identify residues and regions involved in Ca^{2+} activation: the Ca^{2+}-binding event and the transduction of the binding energy through protein conformational changes to the channel domain. The RCK domain model thus provides a framework for the study of Ca^{2+} activation in BK channels.

CHAPTER 1

INTRODUCTION

Ion Channels & Life

Cellular life is defined by the compartmentalization of a set of reactions that transforms energy from the supporting environment (heat, light, chemical bonds) into persistent spatial and temporal order. To do this, cells have evolved means of storing energy harvested at one moment in time to be made available at a later time. Cellular energy is stored in chemical bonds (e.g., ATP) and in potential gradients across membranes. Gradients of ionic species are particularly powerful, being both chemical and electrical in nature. The machinery of the cell responsible for ion trafficking are ion channels and transporters. These are integral membrane proteins that facilitate the passage of ions from one side of the membrane to the other. Ion transporters utilize cellular energy (chemical or gradient) to actively shuttle ions across the membrane, and are thus capable of establishing ion gradients. Ion channels, on the other hand, are passive devices and form transmembrane pores that allow the selective conduction of ions down their electrochemical gradient.

The most extensively studied ion channels to date are those belonging to the family of potassium ion channels, or K^+ channels. These are interesting channels to study because of their ubiquitous expression from bacteria to mammals where they are involved in various processes ranging from the regulation of osmotic pressure in a single cell to the electrical response in muscle fibers to the generation of action potentials in neurons. Despite this broad diversity, all K^+ channels share remarkable core sequence similarity implying strong evolutionary pressure to conserve the structures needed to selectively

pass potassium ions across cell membranes. The diversity of K^+ channel function is accounted for by variable domains N- and C-terminal to the channel's core. These domains confer voltage- and ligand-dependent regulation on the opening and closing, or gating, of the channel (Fig. 1). K^+ channels display a variety of ligand-binding domains, for example, that allow different intracellular factors to regulate K^+ flux. The lack of sequence similarity among these domains suggests that their common regulatory role is a result of convergent evolution. One can imagine various binding domains independently merging with K^+ channel domains over the course of evolution to produce the varied pool of eukaryotic K^+ channels observed today.

BK Channels & Physiology

An interesting subfamily of K^+ channels is the BK channel family (BK for Big K^+ conductance). This is a vital class of ion channels found throughout the animal kingdom and expressed in almost every cell type. Interesting biophysical properties of BK channels include its large conductance and its dual sensitivity to both voltage and intracellular calcium ion (Ca^{2+}) (Horrigan and Aldrich, 2002; Lingle, 2002; Magleby, 2003). Micromolar concentrations of Ca^{2+} *activate* the voltage-dependent gating of BK channels. Not surprisingly, these interesting properties are what make BK channels physiologically unique. This important class of K^+ channel is known to be critical to the function of smooth muscle, spermatocytes, and specialized neurons. As an example of the physiological function of BK channels, consider their localization in presynaptic nerve termini where they play a central role in controlling the release of neurotransmitter (Wang et al., 2001). When an action potential reaches the terminal of a neuron, voltage-

dependent Ca^{2+} channels open and allow an influx of Ca^{2+} to stimulate vesicular fusion and neurotransmitter release. The increase in intracellular Ca^{2+} however also activates BK channels that promptly repolarize the membrane potential with a huge outward conductance of K^{+}. BK channel function thus serves as a negative feedback for Ca^{2+} influx by repolarizing the membrane and closing the voltage-sensitive Ca^{2+} channels, ultimately limiting the release of neurotransmitter. BK channels have in fact been shown to specifically colocalize with Ca^{2+} channels in various neuronal cell types, allowing rapid activation of BK currents (Roberts et al., 1990; Robitaille et al., 1993; Marrion and Tavalin, 1998). As another example, consider the distribution of BK channel splice variants in cochlear hair cells. Sensory hair cells are electrically and mechanically tuned to resonate and respond to particular sound frequencies. Interestingly, the number and kinetics of BK isoforms partially determine the characteristic frequency of a given hair cell, helping to establish the tonotopic map of frequency discrimination (Wu and Fettiplace, 1996; Rosenblatt et al., 1997; Ramanathan et al., 1999). The Ca^{2+}-activation mechanism underlying the varied physiological functions of BK channels is not well understood. We can begin to understand the complexity of the mechanism by examining the structure and function of BK channels.

Structure and Function of the BK Channel

The first structural gene of a BK channel was derived in 1991 from the *slowpoke* (*slo*) locus of *Drosophila melanogaster* (Atkinson et al., 1991). The cloning and sequencing of this gene indicated a large protein of over 1000 amino acids of which only ~220 share sequence similarity to known proteins. The region of similarity corresponds

to the essential components of voltage-gated K^+ channels: a series of six transmembrane helices (S1-S6), a pattern of conserved positively charged residues on S4, and a K^+ channel signature sequence spanning S5 and S6. N-terminal to this region is a unique transmembrane segment (S0); and C-terminal are the remaining ~800 residues, containing four additional hydrophobic segments (S7-S10) and a conspicuous stretch of aspartic acid residues, suggesting a potential Ca^{2+}-binding site (referred to as the Ca^{2+} bowl). These various regions and features are shown in a linear schematic to scale with the primary sequence (Fig. 2). Subsequent characterization of the BK channel expressed in *Xenopus* oocytes, established it as the primary unit of large-conductance, Ca^{2+} activated K^+ currents (Adelman et al., 1992). Homologs of the *Drosophila* BK channel* have since been identified in numerous mammalian genomes, including mouse and human, and in *C. elegans*, sharing over 50% sequence identity (Pallanck and Ganetzky, 1994; Wei et al., 1996).

A significantly divergent member of the BK family was isolated in 1998 from a second locus within the rat genome, *slack* or *slo*2 (Joiner et al., 1998). Slo2 channels function with a much smaller single-channel conductance and respond variably to Ca^{2+} (Yuan et al., 2000). These proteins, however, are capable of forming heterotetramers with Slo1 subunits resulting in intermediate-conductance channels that are Ca^{2+} activated. This observation suggests a possible biological mechanism to control the conduction and activation of BK channels by independently controlling the expression levels of Slo1 and Slo2 channel subunits (Joiner et al., 1998).

---

* Homologs of the original *Drosophila* BK channel are at times referred to as Slo1, Maxi-K, $K_{ca}1.x$, or verbosely, as large-conductance Ca^{2+}-activated K^+ channels; other BK family members include Slo2 (a.k.a., Slack, $K_{ca}4.x$, or IK for intermediate-conductance K^+ channel) and Slo3 (a.k.a., $K_{ca}5.x$ or large-conductance pH-sensitive K^+ channel).

Also in 1998, yet another gene was isolated and identified as a member of the BK family, *slo*3 (Schreiber et al., 1998). Highly similar to Slo1, the most notable difference in the Slo3 paralogs is that they lack the well-conserved stretch of aspartic acids in the far C-terminus, known as the Ca^{2+} bowl. Significantly, Slo3 channels also lack sensitivity to Ca^{2+} and are, instead, sensitive to pH. The coincidence of the Ca^{2+} bowl and Ca^{2+} sensitivity has been the focal point of numerous mutagenesis and chimera studies directed at understanding the basis of Ca^{2+} activation in BK channels.

A thorough mutagenesis study of the Ca^{2+} bowl was performed using the mouse BK channel, mSlo1 (Schreiber and Salkoff, 1997). The effect of mutation was measured by injecting cRNAs *in vitro*-transcribed from mutagenized constructs into *Xenopus* oocytes and assaying the expressed channel currents. A series of mutations within the Ca^{2+}-bowl sequence, DDDDDPD (residues 897-903 in mSlo) demonstrated that two of the aspartic acid residues in particular produced the majority of the effects observed. The first aspartic acid position, D897, decreased Ca^{2+} sensitivity in channels when mutated to ALA, LYS or ASN, or deleted, while having no effect when conservatively mutated to GLU. The second position, D898, when mutated to ASN or deleted caused a significant shift in the Ca^{2+}-activation property of the channel relative to wild type, decreasing the activation by Ca^{2+}. The distinction between mutations that affect *Ca^{2+} sensitivity* versus *Ca^{2+} activation* is based on their distinct response at "saturating" Ca^{2+} concentrations (1mM) as intrepreted by the authors of the original work. They do not claim to have measured Ca^{2+} binding, but rather offer the distinction as a possible explaination for their observations. When these two positions were mutated

or deleted together, the effect of the second position dominated and a decrease in Ca^{2+} activation was observed.

Another important study of the mechanism of Ca^{2+} activation, implicated not only the Ca^{2+} bowl, but also the C-terminus in general (Schreiber et al., 1999). Chimeras of the mouse paralogs, mSlo1 and mSlo3, were formed to demonstrate the functional role with respect to Ca^{2+} activation of various segments of the far C-terminus, or so called *tail* of BK channels. The tail region consists of the final ~400 amino acids (including the Ca^{2+} bowl) and is separated from the N-terminal *core* by a long, variable stretch of sequence (refer to Fig. 2). The core and tail regions do not correlate with the topological separation of domains (i.e., integral membrane domains and intracellular domains), but are instead defined by their functional separability. This separability was demonstrated by the reconstitution of functional, wild type-like channels from the co-injection of independent core and tail constructs into the same oocyte. Furthermore, the core and tail from different homologs were also shown to assemble into functioning channels. Recall that Slo3 channels lack the conserved Ca^{2+}-bowl sequence and are insensitive to Ca^{2+}. The significance of this correlation was dramatically confirmed when the mSlo3 tail was co-injected with the core of mSlo1 and the resulting channels turned out to be completely Ca^{2+} insensitive. Segments of mSlo1 tail sequence were then spliced into the tail construct, replacing analogous segments of mSlo3 sequence. Co-injections of mSlo1 core with various chimeric tail constructs were assayed for restoration of Ca^{2+} sensitivity. Replacing a segment of 34 amino acids centered on the Ca^{2+} bowl (referred to as *region B*) from mSlo1 restored the majority of the native Ca^{2+}-sensitivity range (~60% of ΔV_{50} in 4-300μM Ca^{2+}). The additional replacement of another 35 amino acids immediately

following the Ca^{2+}-bowl segment (*region C*) further restored Ca^{2+} sensitivity. The results clearly demonstrate the importance of the Ca^{2+} bowl and additional C-terminal sequence in the Ca^{2+}-activation mechanism.

The C-terminal tail region is not only important for Ca^{2+} sensitivity, but is also crucial for functional expression of BK channels. Attempts to express the core of various BK channels without a tail region have all failed to produce currents (Wei et al., 1994; Meera et al., 1997). In exception, a recent report states that the removal of the entire C-terminus, from the end of S6 onwards, results in wild type-like BK currents with normal voltage and Ca^{2+} dependence (Piskorowski and Aldrich, 2002). The significance of this finding, however, is obscured by a number of issues addressed in Appendix C. More conservative deletions and mutations within the C-terminus of BK channels have been shown to severely disrupt assembly and function (Wood and Vogeli, 1997; Quirk and Reinhart, 2001). In one study demonstrating the importance of an intact C-terminus, function was restored to full length channel constructs with deleterious deletions within their tail region by the co-injection of native tail constructs (Wood and Vogeli, 1997). The assembly of core and tail constructs thus served as the basis for a complementation study. For example, deletion of the N-terminal half of the tail region abolished channel current expression. With the co-injection of a functional tail construct, however, current expression was restored. A deletion of only ten residues within the C-terminal half of the tail region also eliminated currents and was complemented with a co-injected tail. While the deletions demonstrated the importance of C-terminal sequence, the complementation by co-injection further established the C-terminal region as a critical domain of BK channel function. Interestingly, deleterious deletions and point mutations at the C-

terminal end of the core region could not be complemented by a tail construct with an N-terminal extension covering the mutated sequences. This result demonstrates that the functional boundaries of constructs are not arbitrarily defined; that complementing pairs of co-injection constructs are not trivial, but instead are likely to be constrained by structural factors (both secondary and tertiary) and interfacial elements. Indeed, the boundary between core and tail domains remains the only example of a functional boundary in the current BK literature. Clearly, structural information is needed to fully understand the function of the C-terminus in Ca^{2+}-activated BK channels.

Overview

My thesis is the presentation of a structure-based approach to the study of BK channels with the goal of providing a structural and functional model of the Ca^{2+} activation mechanism. In the next chapter, I present an analysis of BK channel sequences and derive a primary domain model. The model serves as a template for the design of expression constructs in a biochemical study of BK channel domains. Despite the lack of direct structural information (efforts have yet to produce diffracting crystals), the results from this study demonstrate significant features of the structure, assembly and function of the C-terminus. I then introduce prokaryotic homologs of BK channels and develop a homology model. The prokaryotic sequences provide significant diversity to the multiple sequence alignments and highlight critically conserved positions, defining a novel family of domains termed RCK domains. The sequence conservation is given structural meaning when I present the crystal structure of the first RCK domain from *Escherichia coli* that we solved. Using information from the structure in conjunction with

information from the sequence alignments, I propose a detailed secondary and tertiary structural model for the RCK domains of BK channels. The relevant assembly of RCK domains into a quaternary structure is suggested by the crystal structure of the homolog from *Methanobacterium thermoautotrophicum*, MthK. The chapter ends with a model for the general structure and function of RCK domains.

I begin chapter 3 with a detailed analysis of the RCK domain model as it applies to BK channels. The analysis directly results in hypotheses to be tested by electrophysiological experiments presented in this chapter. These experiments include the assay of a series of (1) loop deletions defined by the alignment of BK sequences in the context of the RCK domain model, (2) co- and tri-injections of BK constructs, testing functional domain boundaries and domain assembly, and (3) point mutations probing structural features, interfaces, and Ca^{2+}-binding residues predicted by the RCK domain model. The general agreement between the structural model and functional assays is clearly demonstrated by the results of these varied experiments. The third chapter ends with a discussion of how a Ca^{2+}-induced rearrangement of RCK domains in BK might serve as a model for the function of these domains as mediators of the Ca^{2+}-activation mechanism.

In the fourth chapter, I present a final set of experiments aimed at determining the nature of the connection between the assembly of RCK domains in BK and channel gating. The results of a series of insertions and deletions into the covalent linker connecting the RCK domains to the pore-forming domain suggest a role for the linker in the transduction of Ca^{2+}-induced conformational changes within the RCK domains to the gate of the channel.

The fifth and final chapter is a summary and discussion of the results pertaining to the RCK domain model of the Ca^{2+}-activation mechanism in BK. Mapping relevant mutational data, presented here and in the literature, on the RCK domain model illustrates the remarkable utility of the structural model in interpreting data relating to BK channel function. The thesis concludes with a discussion of the relevance of the presented Ca^{2+} activitation model to the study of this important family of K^+ channels.

CHAPTER 2

BK Sequence Analysis

While the great majority of BK channel sequences share high sequence identity and redundancy there are a few examples that represent divergence in evolution. A multiple sequence alignment of the most diverse members of the BK family immediately highlights regions important to the common structure and function of the family (Appendix A). Of particular importance is the conservation of hydrophobic residues that cluster in the interior of the native protein structure, giving tertiary structure to the string of alpha helices and beta strands. The C-termini of aligned BK sequences contain long stretches of conserved hydrophobic patterns indicative of non-random, structured regions. These stretches of conservation are separated by highly variable regions that vary not only in amino acid character but also in length. These observations lead to a mapping of the primary domain structure for the C-terminus of the BK family. In figure 3A, patterns of hydrophobic conservation are indicated as domains by solid bars underlining the representative sequence alignment. The alignment begins at the signature sequence between the last two transmembrane segments of the channel domain in light gray. Following the channel domain is the first set of C-terminal domains (dark gray, rows 1-3). A highly variable region then separates this set from the second set of domains (rows 5-8). The primary domain structure of the entire human BK sequence is represented to scale with its primary sequence below the alignment (Fig. 3B). Anticipating a correspondence between the primary domain structure and the actual 3-dimension

structure, this domain map was used in the design of constructs for expression and purification.

Expression of BK Constructs

In addition to testing the expression of the entire C-terminus, a number of attempts were made to identify subsets of domains that would express, purify and crystallize to give structural information in parts. Four example constructs, A-D, are shown in relation to the primary domain structure of the human BK C-terminus (Fig. 4A). These constructs are clearly defined by the domain map, each containing a complete domain or set of domains. Using a bacterial expression system, constructs A-D were successfully over-expressed in *E. coli*, as indicated by extracted samples run on SDS-PAGE (Fig. 4B). The expressed proteins segregated into insoluble fractions and were not solubilized by Tris-buffered solutions over a broad range of salt concentrations, nor by the addition of $CaCl_2$, reducing agent, or mild detergent (see Methods). Construct G, shown in figure 5A, consists of the last set of domains that includes the Ca^{2+}-bowl region. Independently, a similar construct was shown to bind Ca^{2+} in an overlay protein blot assay (Bian et al., 2001). With construct G we obtained soluble protein that was readily purified by affinity chromatography and ion exchange on a MonoQ column (Fig. 5B). On a gel filtration column, the 20kDa protein produced a major peak at approximately 120kDa* and a shoulder of additional peaks as high as 240kDa, indicating a range of

* Retention time for gel filtration, or size exclusion chromatography, only roughly correlates with the mass of a protein; it is more precisely a measure of the effective radius of a tumbling, globular protein. The masses indicated here are based on protein standards run under similar conditions. The suggestion of oligameric states is solely based on the observation of elution peaks corresponding to masses significantly greater than the expected mass of the monomer.

oligomers spanning 6 to 12 subunits (Fig. 5C). Noting the tetrameric nature of K^+ channel domains, it was interesting to see oligomerization of a C-terminal region, suggesting that the protein was forming competent structures and interfaces. However, the high order and spread of oligomeric states and tendency towards aggregation indicated that the construct was not optimal. Indeed, limited proteolysis of protein G specifically demonstrated rapid digestion of the entire N-terminal domain, suggesting that perhaps the full set of domains of the tail (see construct M in fig. 6) were required to complete the structure of this region and provide stability. Nevertheless, crystallization conditions were extensively screened with concentrated protein G collected from the major peak of gel filtration runs. The protein demonstrated a great propensity for disorderly precipitation and crystals were not formed.

Due to the high degree of insolubility of human BK constructs expressed in *E. coli*, we turned to a baculovirus system for expression in SF9 insect cells. Construct B was produced as soluble protein in SF9 cells and enhanced by affinity chromatography (Fig. 6B). We also tested the co-expression of constructs that together composed the entire set of C-terminal domains. Constructs B and M, for example, efficiently contain all the domain regions of the C-terminus by excluding the large variable regions: the linker between the two major sets of domains (45 residues) and the sequence following the last domain (58 residues). Remarkably, the co-expression of constructs B and M remedied a number of problems (Fig. 6B). For example, the purification of protein M by itself was hindered by the fact that its purification tag was being cleaved by endogenous proteolytic activity prior to affinity column binding. When co-expressed with B, however, the tag-less protein M would co-purify with the tagged protein B in an approximate 1:1 ratio. In

addition, the B+M complex was more stable than B alone during further purification. The co-purification indicated the existence of complementary interfaces within B and M that allow assembly. These same interfaces, left unmatched, may be responsible for the aggregation and precipitation of partial constructs expressed alone. The B+M complex produced a number of peaks on a gel filtration column: a broad peak consistent with dimers of B+M complex, a peak suggesting a higher-order oligameric state of the complex (consistent with an octamer), and an aggregate peak consisting of excess B (Fig. 6C). Taking the "dimer" complex peak and running it again on gel filtration reproduced the "octameric" complex peak, demonstrating the equilibrium between these states of the complex (Fig. 6D). Again, the observation of oligomeric states was intriguing and encouraging when considered in the context of the associated tetramer of channel domains in the native protein. Contrasting the quality of the oligomeric peaks with those of protein G or with the aggregation of protein B, the B+M complex is clearly a better behaving protein. B+M is also a more complete protein, representing the full set of C-terminal domains. The purified complex, however, did not yield crystals in crystallization trials, precipitating in most conditions.

A tri-expression was attempted with the three components, B, N, and G, which together composed a complete set of domains. The constructs maintained purification tags and together were purified on an affinity column (data not shown). The excess of certain components produced a series of overlapping peaks on gel filtration. Significantly, one of the peaks corresponded to the complex of B+N+G as determined by size estimation and SDS-PAGE, demonstrating a novel domain boundary and additional domain interfaces. However, due to the lack of control over stoichiometry, the

expression of multiple components was overall an inefficient way to produce and purify the C-terminal domains.

As an alternative, construct L* was designed to consist of the entire set of C-terminal domains in a single construct and was expressed as soluble protein in SF9 (Fig. 7). Elutions from the initial purification step showed a collection of protein species co-purifying (Fig. 7B). The associated species corresponded to the full-length protein and various smaller fragments representing cleavage products from endogenous proteolysis. Further purification with ion exchange did not improve the homogeneity of the sample. On a gel filtration column, this collection of proteins ran as a single species at a mass approximating a monomer of the full-length protein. The proteolyzed fragments were assembling to form proteins that ran at the same effective size as full-length protein L. While the assembly of fragments was reminiscent of proteins B and M, the behavior of the protein L species on gel filtration was significantly different. The effective size of protein L indicated by gel filtration suggested a monomer and was more homogeneous than that of the B+M complex. Interestingly, the state of protein L was dependent on Ca^{2+} In the presence of Ca^{2+}, the elution profile suggested a significantly larger effective radius and an oligameric state (Fig. 7C). The effect of Ca^{2+} on the gel filtration profile for protein L demonstrates a response to Ca^{2+}. This is what you would expect from a protein responsible for a Ca^{2+}-dependent process: a conformational change or change in oligameric state in response to binding Ca^{2+}. These gel filtration results thus provided an assay of function for the purified domains, suggesting their importance in a Ca^{2+} activation mechanism.

---

* Construct L is different from D in that it excludes the last 58 residues of protein; the construct is different from B+M in that it includes the major linker of 45 residues.

The behavior of proteins expressed from the primary domain model of the human BK C-terminus gave important demonstrations of the structure and function of the C-terminal domains. Properties of structure, stability and assembly were found to be unique to a complete C-terminus, whether encoded in a single construct or in co-expressed constructs. Furthermore, the gel filtration results suggest that the full set of domains responds to Ca^{2+} with some sort of conformational change or change in oligameric state. These results were an encouraging indication of the potential of these domains to transduce a Ca^{2+}-binding event into a mechanical force generated by a change in conformation. While this approach of direct biochemical and structural study of the human BK C-terminus has yet to yield a crystal structure, it continues to be actively pursued in the lab. In parallel to these ongoing efforts, a homology model was developed based on the study of prokaryotic homologs of BK. Structural information from prokaryotic homologs significantly refined the model of domain structure and function for the BK C-terminus.

Prokaryotic Homologs and the RCK Domain

The existence of prokaryotic homologs of BK has previously been reported (Stumpe et al., 1996; Durell et al., 1999). Though not explicitly noted, the relatedness between a prokaryotic K^+ channel and BK channels was even indicated in the alignment statistics presented in the initial paper reporting the sequence and cloning of the first prokaryotic K^+ channel, *E. coli* kch (Milkman, 1994). The sequence similarity between these distantly related proteins extends beyond the canonical channel domain, indicating a significant conservation of C-terminal domains. Numerous examples of prokaryotic

K^+ channels have since been identified in the sequencing of microbial genomes. While prokaryotic K^+ channels are related to eukaryotic K^+ channels in general by the conservation of K^+-channel motifs, the majority of them are further related to BK channels by the conservation of the same C-terminal domain found on the *E. coli* channel. This domain, in fact, is ubiquitous in prokaryotic K^+-channel and K^+-transporter sequences (Derst and Karschin, 1998). Based on their exclusive association with K^+ conducting systems we termed them RCK domains, for their presumed role in Regulating the Conduction of K^+ (Jiang et al., 2001).

While in most instances only a single RCK domain is encoded following the channel domain, there are a few cases where a second RCK domain is present in the same gene (Fig. 8A). Such pairs of RCK domains are either found on the N- and C-termini of a given channel sequence or they are found in tandem, C-terminal to the channel. As is shown in figure 8B, this latter arrangement describes the domain structure of the eukaryotic BK channel, where two RCK domains follow the channel-forming region (S0-S6).

The addition of prokaryotic RCK domain sequences significantly enhanced the diversity of the multiple sequence alignment of BK channel sequences. While the alignment was powerful in showing a significant pattern of conservation, implying conserved structure and function, direct structural information was needed to translate the 1-dimensional alignment into a secondary and tertiary structural model. This information was provided when we solved the first RCK domain structure from *E. coli* kch (Jiang et al., 2001).

The *Escherichia coli* channel, kch, is a six transmembrane K^+ channel with a C-terminal RCK domain. The RCK domain was expressed, purified and crystallized. The structure was determined by means of a multiwavelength anomalous dispersion experiment and refined to 2.4Å. The crystal structure of the *E. coli* RCK domain revealed an α-β-α layered topology consisting of a six stranded beta sheet sandwiched between five alpha helices forming a well-defined hydrophobic core. The topology also provides a versatile binding cleft at the C-terminal ends of the beta sheet. In other examples, this cleft binds a variety of ligands: ions, nucleotides, NAD(+) and other small molecules. Two alpha helices (αF and αG) follow the α-β-α layered region of the RCK domain in a helix-turn-helix motif that participates in one of two major domain interfaces. A second interface is formed by hydrophobic residues lining the external face of αD. The two interfaces generated a long chain of linked RCK domains in the crystal structure that did not terminate or close to form a ring. Despite the impossibility of these RCK polymers occurring naturally, it was clear that the interfaces were relevant to RCK assembly as they were both observed in each of two different crystal forms and well conserved in all RCK sequences, including those from the most distant BK sequences.

The *E. coli* RCK crystal structure gave form to the aligned RCK sequences; the pattern of sequence conservation could now be explicitly understood in terms of structure. An alignment of RCK sequences covering the initial segment of the domain (from βA to αD) illustrates the structural perspective provided by the *E. coli* RCK structure (Fig. 9). There is the fundamental conservation of secondary elements and tertiary structure: the hydrophobic pattern for alternating alpha helices and beta strands that conform to a layered topology. The tertiary structure is further defined by the

conservation of glycine and proline residues in positions requiring acute backbone angles and of acidic and basic residues in positions that interact to form salt bridges. And quaternary structure is indicated by the strict conservation of unique hydrophobic residues that participate in domain interfaces responsible for the assembly of RCK domains. The conservation of detailed tertiary and quaternary structure in the context of the exclusive association with K^+ channels and K^+ transporters strongly suggests a common mode of function. RCK domains, thus defined by the conservation of sequence underlying these structural features, represent a unique family of domains with common structure and function.

The full picture of the RCK domain assembly was seen in the crystal structure of another prokaryotic homolog, MthK, determined by other members of the lab (Jiang et al., 2002). From *Methanobacterium thermoautotrophicum*, the MthK channel is a two transmembrane K^+ channel with a single, C-terminal RCK domain. The full-length MthK protein was overexpressed in *E. coli* and purified by affinity chromatography. Following crystallization, the structure of the MthK channel was solved using X-ray diffraction data collected on native protein crystals and heavy atom derivatives. A 3.3Å structure of the two-transmembrane channel and associated RCK domains was the first structure of an ion channel with its ligand-gating domain intact. The structure revealed a total of *eight* RCK domains forming an octameric ring on the intracellular side of a tetramer of channel domains. Additional RCK domains were generated from the MthK gene by a second start site downstream of the channel domain, just preceding the RCK domain. The production of additional, free RCK domains was also observed in the expression of other prokaryotic K^+ channel genes containing RCK sequence, including kch from *E. coli*.

Alternatively, a second set of RCK domains may be provided by genes encoding isolated RCK domains observed in many prokaryotic genomes, and, as previously mentioned, there are a few cases where a pair of RCK domains are encoded in the same gene, explicitly providing the 2:1 ratio of RCK domains to channel domains. The assembled ring of RCK domains in MthK utilizes the same protein-protein interfaces observed in the *E. coli* kch RCK structure. The ring assembly in MthK, therefore, may represent the quaternary structure conserved in all RCK sequences.

The structure also revealed a Ca^{2+} ion bound to each RCK domain. Complementary to this observation, functional analysis of reconstituted MthK channels in lipid bilayers demonstrated the activation of MthK gating by Ca^{2+}. Thus, it was proposed that the octameric assembly of RCK domains functions as a ligand-gating domain in which upon binding Ca^{2+}, the rearrangement of RCK domains induces channel gating. Though the details of the RCK domain rearrangement are unknown, a basic model was presented based on the comparison of the two interfaces found in the MthK and *E. coli* kch RCK domain structures. The relative orientation of a given dimer around the interfaces on the external face of αD is proposed to be fixed, while the orientation with respect to the interface formed by αF and αG is variable. The variability implies flexibility at this site, and suggests a possible pivot or hinge position. Furthermore, the Ca^{2+}-binding sites are in close proximity to this flexible interface; in fact, the two Ca^{2+} ions bound in each dimer around this interface are separated from one another by a single phenylalanine side chain positioned at the proposed hinge point. The proximity of Ca^{2+} to the flexible interface suggests a direct interaction, connecting the Ca^{2+}-binding event to domain movements around the flexible interface. As the RCK domain immediately

follows the last TM helix of MthK that lines the pore and serves as a gate to ion conduction, ligand-induced rearrangements within the octamer of RCK domains would reasonably influence channel gating.

The RCK structures from prokaryotic homologs provided structural insight into the otherwise abstract pattern of sequence conservation, refining the domain model to a level of secondary, tertiary and quaternary structure. The *E. coli* structure demonstrated not only the hydrophobic pattern fundamental to the protein fold, but also additional structural constraints (GLY/PRO positions and salt bridges) and features that indicated domain assembly. The MthK structure revealed the precise RCK domain assembly and demonstrated the same structural constraints and features observed in the *E. coli* structure. The MthK structure also suggested a functional model for RCK domains, where the assembled domains could undergo a conformational change via flexible interfaces in response to ligand binding, transducing the binding event into a mechanical force positioned to influence channel gating. Thus, by adding structural information to the analysis of sequence we have generated a hypothetical structural and functional model for all RCK domains. This is the first model to be proposed for the complete set of C-terminal domains in BK. A thorough test of the model will show how the structure and assembly of BK domains is consistent with the proposed RCK domain structure and how the hypothesis for RCK domain function may relate to the mechanism of Ca^{2+} activation. First, we consider the alignment of BK sequences with the prokaryotic homologs in more detail. With the structural information provided by prokaryotic RCK domains, the alignment directly implies structural constraints and features in BK that are testable by electrophysiology and a variety of mutagenesis approaches.

CHAPTER 3

RCK Sequence Analysis

The results of a multiple sequence alignment of ~100 RCK domains from prokaryotic K^+ channels, K^+ transport systems and the eukaryotic BK family of K^+ channels are represented on a few key sequences for simplicity in figure 10A (Appendix B). The pattern of conservation in blue is thus representative of all the available low-redundant sequence information. The first and second lines of the alignment are the first and second RCK domains of the human BK channel (HBK), respectively. The next three lines are representative prokaryotic homologues with known 3-dimensional structure: MthK, KtrA (Roosild et al., 2002), and *E. coli* kch. The last line of the alignment indicates the correspondence of secondary structure from the MthK crystal structure with the aligned sequences. Notice that the conservation in blue clusters over regions of structure in a pattern of alternating beta strands (solid hydrophobic stretch) and alpha helices (hydrophobic positions every 3-4 residues), suggesting a beta sheet buried by alpha helices in an α-β-α layered topology. Additional hydrophobic positions indicated by green, orange and red correspond to residues that make up domain interfaces. Residues of the fixed interface at αD are indicated by green. Residues on αF and on the interfacing beta sheet (βA-βE) are indicated by orange, while those on αG and its interfacing beta sheet (βF-βI) are indicated by red. The structures rendered below the alignment maintain the same color coded residues and illustrate each of the two interfaces (Fig. 10B-D). The fixed interface (Fig. 10C) involves the αD helices from two interfacing domains. The flexible interface (Fig. 10D) consists of a pair of alpha helices

(αF and αG) from each of two domains packing against the major beta sheets of the other domain, resembling a domain swap of two helices. The conserved interfaces generate an octameric ring assembly of RCK domains (Fig. 11). Other conserved positions in the alignment include glycine and proline residues, and acidic and basic residues involved in salt bridging interactions (e.g., the positions of K448 and D481 in HBK).

Loop Deletions

The RCK sequences from HBK maintain the conserved positions and are indistinguishable from other sequences in the alignment based on the degree of conservation. The eukaryotic BK family sequences do, however, contain additional stretches of sequence not observed in prokaryotic sequences. These stretches are identified in the alignment as insertions relative to the prokaryotic sequences. Each of the insertions consists of highly variable sequence, lacking conservation even within the BK family of sequences. Indeed, the largest of these insertions are the same variable regions identified during the analysis of BK channel sequences in determining the primary domain structure. In the alignment of RCK domains, the insertions are localized to loop regions between secondary structural elements. It is therefore reasonable to hypothesize that these loop insertions consist of extraneous sequence, residues that do not contribute to higher-order structure. Each loop region of significant length in the human BK sequence was individually deleted from constructs tested for current expression and function in *Xenopus* oocytes. Of the eight deletion constructs tested, seven expressed wild type-like levels of functioning BK channels. The corresponding loops from these

seven constructs have been replaced in the alignment shown in figure 10A by a red, parenthesized number representing their length.

The loops are also represented along a schematic of the RCK domain model of HBK adjacent to the schematic of the primary domain model determined from the alignment of only BK channel sequences (Fig. 12A). Notice that the larger loops (Δ16, Δ45, Δ42, Δ34 and Δ58) all correspond to the variable regions identified in the primary domain structure. This correspondence demonstrates the coarse agreement between the two domain models. Three additional loops (Δ5, Δ6 and Δ10) were identified in the refined RCK domain model. Below the schematic, the sequences of the attempted loop deletions are listed. The C-terminus of HBK is ~800 residues in length. Some of these deletions individually represent 2-7% of the entire C-terminus. Contrasted with the importance of a complete, intact C-terminus demonstrated by previous expression, deletion and mutation results, the fact that only one of these alignment-based loop deletions had an impact on the expression of functioning BK channels is remarkable. The effects of loop deletion are visible in the current recordings (Fig. 12B). The assay of these currents was mostly binary: a deletion construct either produced current or it did not. The observation of significant channel current was therefore sufficient to define the deleted region as nonessential sequence, here referred to as a loop. It was further noted that the majority of the tested loop deletions had little to no effect on the voltage and Ca^{2+} dependence of the channel. The first set of traces (boxed) shows voltage-dependent activation and deactivation (inset) of wild type human BK channels in 10μM Ca^{2+}. The remaining eight traces labeled by the length of the deletion correspond to the loop deletions listed in figure 12A. Currents from the three largest deletions, Δ45, Δ58 and

Δ42, and from Δ6 are basically indistinguishable from wild type in terms of expression level, kinetics, and voltage- and calcium-dependence. G-V curves for these loop deletions are shown in solid symbols overlapping the wild type curve (Fig. 12C). Currents from Δ5 and Δ10 show slightly faster activation kinetics and produce slightly left-shifted G-V curves. It is interesting to note that these two loop deletions, having similar effects, are similarly placed in the first and second RCK domains of HBK (between βD and αD), hinting at the symmetry of the RCK domain model. The currents from Δ16 are dramatically different from wild type, having much slower activation kinetics and faster deactivation kinetics. Figure 12C shows the severe right-shifting effect of this deletion on the G-V curve at 10μM Ca^{2+}. The Ca^{2+} activation of wild type G-V curves is contrasted with that of Δ16 over a range of [Ca^{2+}] (Figs. 12D&E). Notice that the G-V curves of Δ16 are not only shifted relative to wild type, but also more closely grouped. The effect of Δ16 is identical to the effect observed in the point mutation of M513I (Bao et al., 2002). M513 immediately precedes the deleted loop (Δ16 is residues R514-L529), thus the basis for the observed effects may be the same. It is also interesting to note that while there is not significant conservation of sequence in the region of Δ16, the length of this loop is similar in prokaryotic sequences that share the tandem configuration of two C-terminal RCK domains present in BK channel sequences (refer to Appendix B). The only deletion that resulted in loss of function altogether in our assay was Δ34. Within BK channel sequences, the region defined by Δ34 does contain a degree of sequence conservation among the Slo1 and Slo3 channels, but is completely absent in Slo2 channels, including those from *L. major* (e.g., L1BK2; Appendix B). Nevertheless, the region of Δ34 proves to play a structural or functional

role in the human BK channel and is therefore not defined here as a loop. Maintaining this stretch of residues in the sequence alignment in figure 10A highlights a weak area of the RCK domain model for the human BK channel. The weakness may be in the alignment of this area, simply requiring adjustment; alternatively, the model itself may not be accurate for this particular area.

Overall the proposed RCK domain model predicted significant regions of extraneous sequence likely to form unstructured loops. A total of 182 residues from the 773 composing the C-terminus of HBK (~25%) were successfully removed in stretches ranging from 5 to 58 residues. This is not a trivial result considering the importance of this region as demonstrated by the truncations, deletions and point mutations of earlier work (Wei et al., 1994; Meera et al., 1997; Wood and Vogeli, 1997; Quirk and Reinhart, 2001). As the loops were defined by the RCK domain model, these results lend support to the model as it applies to the human BK channel.

Co-injections

The proposed model implies a high degree of symmetry between the two RCK domains; they are, in fact, identical in the case of MthK and presumably in many other prokaryotic examples. In addition, the two domains are expected to be able to fold independently and create complementary domain interfaces that allow the assembly of the octameric ring. These are severe constraints for the two C-terminal domains of HBK, which present only a faint sequence similarity to one another (sequence identity is only 10% and similarity ~25% over 400 amino acids). The ability of HBK to conform to these constraints can be tested by co-expression of paired constructs in oocytes.

A co-injection strategy was used to test the expression of functioning BK channels from pairs of HBK constructs independently transcribed into cRNA. The basic idea behind these experiments is to assess whether two parts of the protein can assemble via a protein-protein interface without being covalently linked through the polypeptide chain. It is important to note that in all cases the full complement of protein was required for functional expression. Single components and incomplete sets of domains never produced currents. Dissection points were chosen based on the hypothesized structural model. These positions are indicated by posts numbered 1-14 along the schematic of the RCK domain model of HBK (Fig. 13A). They are also indicated in relation to the sequence of HBK in figure 10A. To test position 10, for example, two constructs were made: one beginning at the native N-terminus and ending at position 10 (a C-terminal truncation), and the other beginning at position 10 and ending at the native C-terminus (an N-terminal truncation) (see Methods: Construct Design and Mutagenesis). Separate cRNAs generated *in vitro* from these two constructs were then injected into the same oocyte. The co-injections were then assayed for macroscopic current expression of BK channels maintaining voltage and Ca^{2+}dependence. The detection of significant channel currents from the co-injection of constructs that do not produce currents when injected alone was sufficient to define the co-injected pair as competent for functional assembly. Results for all the test positions are indicated in a binary manner: position numbers in circles produced currents, while those in diamonds failed to produce significant currents. As indicated by this notation, position 10 is a positive expression co-injection point and therefore represents a functional boundary. Notice that this is equivalent to the boundary separating core and tail domains previously demonstrated by co-injection studies (Wei et

al., 1994; Meera et al., 1997). Using both positions 10 and 11 as alternate stops and starts, respectively, the 45 intervening residues were effectively removed from a set of constructs* (Fig. 13B). Notice also that, in terms of the representation of C-terminal domains, this pair of constructs is equivalent to the pair of SF9 expression constructs, B and M that co-expressed to form a stable, soluble complex. Co-injection in oocytes provided an additional functional assay of equivalent co-expression constructs previously assayed biochemically. We thus confirm that the domains represented by these constructs are capable of assembly and further demonstrate that the assembly is fully functional.

For every successful co-injection pair, each of the two constructs was tested for independent function by injecting cRNAs for each construct into separate oocytes. These control experiments were essentially tests of various N-terminal and C-terminal fragments. None of these fragments produced currents when injected alone. Furthermore, co-injection of pairs of constructs that represented an incomplete set of domains as defined by the primary domain model of BK, also failed to produce current. These results demonstrate that the entire set of domains is required for functional expression in oocytes.

Another set of sites similar to the ones used in generating SF9 expression constructs includes positions 12 and 13 (see constructs G and N), marking the boundaries of the successfully deleted loop, Δ42. A co-injection set of constructs was generated around site 12 in order to assay the position as a functional domain boundary (Fig. 13B). This set of constructs expressed and assembled to produce functioning HBK currents

* The loop deletion Δ45 was in fact tested by the co-injection of this set of constructs.

(Fig. 13D). The fact of this novel functional boundary indicates that interfacial residues on one of the constructs complement those on the other, allowing assembly and function. According to the model, site 12 is located between αD and βE on the second RCK domain of HBK. The symmetrical position on the first RCK domain is site 6. Successful co-injection around site 6 thus implies symmetry in functional boundaries in the two domains of HBK. To set further constraints on the assembly of constructs, two tri-injection experiments were performed (Fig. 13C). The tri-injections use sites 10 and 11 (Δ45) to split the two RCK domains. In addition, one uses site 12, while the other uses the symmetrical site 6. The tri-injections both successfully produced functional BK currents (Fig. 13E). Leaving out any of the three constructs from either set, creating large domain truncations or deletions results in the failure of current expression. This result is the functional analog to the tri-expression of B+N+G in SF9 cells and implies that multiple sets of interfaces serve in the assembly of complete functioning channels. With a detailed model available we can refer to the alignment in figure 10A and identify the specific interfacial elements at work in these two sets of tri-injections. For example, consider the trisection at sites 10-11 and 12. The N-terminal construct is the first RCK domain, fully intact with a complete set of interfacial positions. The middle construct, bounded by sites 11 and 12, contains most of the interfacial positions of the first beta sheet (in orange) and the positions of αD (in green) of the second RCK domain. These elements assemble with the interfacial positions of the first RCK domain: αF (orange) and αD (green). The C-terminal construct contains the interfacial positions of αF (orange), αG (red), and the second beta sheet (red) of the second RCK domain. These assemble with the remaining interfaces of the first RCK domain: the first beta sheet

(orange), the second beta sheet (red), and αG (red). Thus, each construct has at least two interfacial elements. Likewise, a minimum of two interfacial elements is retained by each of the constructs in the symmetrical tri-injection involving sites 10-11 and 6. The success of these experiments demonstrates that the interfaces present on the tri-injection constructs are sufficient in allowing functional domain assembly. In order to test the minimum interface sufficient and necessary for functional assembly, sites 1-9 were considered.

Each of these dissection points occurs in a loop between structured regions (Fig. 10A), except site 8 which dissects the αF-αG interfacial element and served as a negative control. Site 9 cuts after αG, sites 3 through 7 cut after each of the secondary elements from βC to βE, site 2 cuts after βA, and site 1 dissects the channel domain from the entire set of C-terminal domains. Co-injections based on these dissection points established the most N-terminal functional boundary at site 5. Dissection at site 5 maintains most of the interfacial positions (4 out of 5) of the first beta sheet (orange) in the N-terminal construct. These four positions, composing a single interfacial element, are thus sufficient to assemble with the remaining positions on the C-terminal fragment. Dissection at site 4, however, leaves only 2 of the 5 interfacial positions, and assembly fails. Therefore, the two positions on βD prove necessary to the functional assembly of domains.

At the tail end of the second RCK domain, dissection at site 16 generates a C-terminal construct that maintains the second beta sheet interface. This interfacial element is not sufficient for assembly according to the failure of the co-injection to produce channel currents. Dissection at site 13, however, which maintains βE and the αF-αG

element in addition to the second beta sheet in the C-terminal construct, did allow assembly. Dissection at either site 14 or 15 fails, but the co-injection of the N-terminal construct of 15 and the C-terminal construct of 14 produced functioning BK currents. The co-injection produces an overlap in the region between sites 14 and 15. The result thus suggests a functional boundary within that stretch of sequence. This establishes the most C-terminal functional boundary in the set of domains and indicates the necessity of intact αF-αG and second beta sheet interfaces.

The co-injection results demonstrate functional domain boundaries, implying structural domain boundaries. The assay of boundaries was used to test symmetry and assembly in the C-terminal domains of HBK. The results are consistent with the structural model provided by RCK domains. The model reasonably explains the means and limits of the co- and tri-injections by focusing on the interfacial elements and underlying structure responsible for domain assembly. Together with the loop deletion experiments, co- and tri-injections have probed the tertiary and quaternary structure of the HBK C-terminus. The primary domain structure, the inherent symmetry, and the elements responsible for domain assembly are compatible with the RCK domain model. Having examined the general features of the domain model for the C-terminus of HBK, we now focus on the detailed features of the domains indicated by the model. These features are tested by the electrophysiological analysis of a series of site-directed point mutations.

Point Mutations

BK channel gating (the transistion between closed and open states) is regulated by the allosteric effects of voltage and Ca^{2+} which act essentially independent of one another (Cui and Aldrich, 2000; Horrigan and Aldrich, 2002; Lingle, 2002). In the absense of Ca^{2+} (the unliganded state), voltage can open BK channels to maximal open probabilities. The addition of Ca^{2+} in micromolar quantities shifts the voltage dependence toward more negative voltages without altering basic gating properties such as the shape of the G-V (conductance vs. voltage) relationship or the maximum open probability. The analysis of G-V relations collected over a wide range of Ca^{2+} concentration is thus simplified by allowing one to compare G-V curves approximated by a simple Boltzmann equation (see Methods: Electrophysiology; Cox et al., 1997a; Cox et al., 1997b). Additional consideration is required for the treatment and interpretation of effects due to point mutations made in the channel. Mutations in BK can potentially alter fundamental properties of the channel (e.g., single channel conductance or selectivity), or of the gating function (e.g., range of open probability, voltage dependence or Ca^{2+} dependence), complicating and limiting comparative analyses. Based on the observations and assumptions detailed below, the point mutations presented in the remainder of this chapter are considered to primarily affect the Ca^{2+} dependence of BK channel gating and are thus treated as simple shifts in G-V relations by the analysis described above. In support of this simplification, open probabilities were determined by single channel analysis for a representative subset of mutations and a model of independent voltage- and Ca^{2+}-dependent processes was assumed.

Single channel records were collected for specific point mutations in each of the regions investigated: the salt bridge, the αD interface, and the Ca^{2+}-binding cleft. Single channel conductance and range of open probability were unperturbed by mutations within these regions. As an example, consider the substitution K448D, one of a pair of positions predicted to form a salt bridge. Analysis of a single channel at various voltages and Ca^{2+} concentrations demonstrated a range of open probability and single channel conductance identical to wild type channels (Fig. 14A). Furthermore, the treatment of macrocurrents (i.e., the normalization, fitting and parameterization) is validated to a first approximation by the strong correlation of G/G_{max} and open probability determined from single channel records (Fig. 14B). While single channels were not obtained for many of the point mutation presented in the following sections, the maintainance of properties observed in specific representative mutations is assumed to be general.

Over the past 20 years of study of BK channel function an impressive body of work has lead to a robust allosteric model of BK voltage- and Ca^{2+}-dependent gating (Horrigan and Aldrich, 2002; Lingle, 2002; Magleby, 2003). The dual dependency of BK channel gating provides powerful means for studying the gating process. Even more remarkable perhaps is the significant independence of the two mechanisms of gating present in BK. The structural model being proposed here for the intracellular domains of BK, provides an intriguing physical picture of these separate gating mechanisms. The voltage dependence has been localized to the voltage-sensor domain (S1-S4) and its interaction with the pore-forming domain (S5-S6), and is thus confined, for the most part, within the membrane. Here we are presenting a model for Ca^{2+} dependence that is localized to the set of RCK domains on the intracellular side of the channel and its

interaction with the pore-forming domain. The nature of this interaction will be investigated in more detail in Chapter 4, but note for the moment that the RCK domains immediately follow the last transmembrane helix, S6, which lines the pore of the channel and acts as a gate. The direct interaction between RCK domains and the gate could potentially confer Ca^{2+} activation independent of the voltage-dependent mechanism. The independence of Ca^{2+} activation correlates with the isolation of the Ca^{2+}-activation machinery proposed by the RCK domain model. While this correlation cannot be the basis for knowing the underlying effects of mutations within the intracellular domains, it perhaps should not be surprising if such mutations have isolated effects on Ca^{2+} dependence. With the assumption of an independent model I will describe shifts in the G-V curves from mutations within the intracellular domains as increasing (leftward) or decreasing (rightward) effects on the Ca^{2+}-activation of BK channel gating relative to wild type.

Salt bridge

The first set of point mutations was directed at the residues predicted to interact in forming a salt bridge in HBK, K448 and D481 (Fig. 10A). The LYS position was mutated to an ASP (K448D) and the ASP position was independently mutated to a LYS (D481K). Interestingly, these point mutations elicited currents with properties significantly different from wild type. At a given Ca^{2+} concentration, the G-V curves for each of the mutants are significantly right shifted relative to that of wild type, a deactivation of the effect of Ca^{2+} (Fig. 15A). The parameterization of the G-V curves provides the terms z and V_{50}, the effective valence and midpoint voltage, respectively. If

we assume an energetic term, zV_{50}, and the conditions for a thermodynamic double mutant cycle, the null case states the additivity of independent mutations relative to wild type: if the effects of mutation A and mutation B are independent, or energetically uncoupled, then the effect of the double mutation AB will simply be the sum of the two effects ($\Delta zV_{50(AB)} = \Delta zV_{50(A)} + \Delta zV_{50(B)}$). A careful consideration of the conditions under which this expression is valid has been given but have not been rigorously tested here (Yifrach and MacKinnon, 2002). On the other hand, if the sum of the measured effects of the single mutations does *not* equal that of the double mutation, then the mutations are not independent and are said to be energetically coupled. Thus, one can predict the effect of a double mutation if the effects of two independent single mutations are known. Figure 15A shows the predicted G-V curve for the double mutation (K448D/D481K; open diamonds) based on the measured effects of the two single mutations relative to wild type. The actual effect of the double mutation (solid diamonds) is in fact left-shifted relative to wild type, dramatically deviated from the prediction. The two single mutations therefore are not independent; perturbations at positions K448 and D481 are in fact energetically coupled. This finding is compatible with the hypothesis that these positions participate in a salt bridge interaction. The strict conservation of these two oppositely charged positions in the aligned RCK domains was given structural significance by the *E. coli* kch and MthK structures, revealing their interaction in the tertiary structure. The double mutant analysis of these same positions in HBK implies that they are energetically coupled, which supports the modeled structural interaction and further relates structure to function. The fact that mutations to these positions have an effect on Ca^{2+}-activation, as measured by shifts in G-V curves, suggests a correlation

between a uniquely conserved structural feature of RCK domains (the salt bridge) and the role of RCK domains in the Ca^{2+} activation of BK.

Interface

The interfacial elements responsible for domain assembly were tested *en masse* in the co-injection experiments previously described. In order to test the function of one such element in more detail a series of point mutations targeting the αD interface were made. The αD interface, or the fixed interface, is simpler than the flexible interface. The interface primarily involves six hydrophobic residues: three from each of the two interfacing αD helices (Fig. 10C). These hydrophobic positions are particularly conspicuous in RCK domain sequences. Positioned on the outer face of the helix, they break the typical hydrophobic pattern of a helix in an α-β-α layered topology, i.e., every 3-4 residues. Referring to the alignment in figure 10A almost every position around two full turns of αD (6 of 7 residues) is a conserved hydrophobic position in over 65% of the RCK domain sequences. While some of the positions pack into the interior of the protein, three positions (the interfacial positions) stick out away from the protein. Like that of the salt bridge, the conservation of this feature is not common to other structurally related proteins, but rather is exclusive to the family of RCK proteins. Recall that it is, in fact, the combined conservation of interfacial residues, salt bridging residues, and the association with K^+ channels and K^+ transporters that defines RCK domains as a unique family of proteins. Consistent with the special conservation of the interfacial residues of αD, mutation of these residues has significant effects on HBK channel expression and function.

In parallel experiments, wild type and mutated constructs were tested for functional expression in oocytes. Figure 16A shows the results of wild type HBK expression versus that of two double mutations of the αD interface of the RCK domains of HBK. The double mutation, IMAA, involves two of the interfacial residues on αD of the first RCK domain, I441A/M442A. The other double mutation, ILAA, involves the symmetrical pair of interfacial residues on αD of the second RCK domain, I821A/L822A. Each of these double mutations results in a dramatic decrease in the functional expression of HBK channels in oocytes. An analogous construct was made of the prokaryotic homologue, *E. coli* kch, involving the mutation of the lone RCK domain encoded in its sequence (Jiang et al., 2001). Having a native alanine in one of the two analogous positions, a double alanine construct was generated by a single mutation, F327A. The double alanine construct of kch could not be overexpressed in *E. coli* by the same means used to produce and purify biochemical quantities of wild type kch. These results suggest that the highly conserved hydrophobic positions of αD are indeed important to RCK domains, most likely affecting their ability to assemble into a stable, functioning quaternary structure. The mutation of interfacial residues by alanine substitution has a significant affect on the competency of the interface.

Single mutations of the third interfacial residue on the αD helices had more subtle effects on the functional expression of HBK in oocytes. In the HBK sequence these residues are I445 in the first RCK domain and L825 in the second. The mutation of I445 to alanine or leucine resulted in wild type levels of current expression with significantly right-shifted voltage dependence (Fig. 16B). Mutation of the symmetrical position, L825, to alanine or methionine also resulted in macrocurrents with a right-shifted

response. Interpreting these mutational effects as deactivating effects on the Ca^{2+} activation mechanism we can then speculate as to the mechanism. Perhaps by disrupting the fixed interface between αD helices the rigidity of the RCK domain assembly is compromised, altering its ability to transduce Ca^{2+}-binding energy into an effective conformational change. The resulting decrease in transduction might then appear as a decrease in Ca^{2+}-activation and a right shifting of G-V curves.

Ca^{2+} binding

Many of the effects on Ca^{2+} activation discussed so far have involved intermediate steps along the energetic pathway from the initial Ca^{2+}-binding event to the ultimate influence on channel gating. According to the RCK domain model and supporting evidence, these intermediate events include a conformational change in the assembled RCK domains that energetically involves many structural elements such as salt bridges and domain interfaces. Let us now consider in detail the first event of the Ca^{2+}-activation mechanism: Ca^{2+} binding. The first stretch of sequence within the ~800 amino acid C-terminus of BK channels to capture the attention of investigators was DQDDDDDPD, not surprisingly. This conspicuous series, rich in aspartic acids and aptly named the Ca^{2+} bowl, held the promise of immediately elucidating Ca^{2+} activation in this important family of K^+ channels. The correlation between the Ca^{2+} bowl and Ca^{2+} sensitivity was made significant by the discovery of the Slo3 variant of the BK family, which despite high sequence identity with Slo1, lacked both the Ca^{2+} bowl sequence and Ca^{2+} sensitivity (Schreiber et al., 1998). Numerous studies, as previously discussed, have demonstrated the importance of the Ca^{2+} bowl and surrounding sequence of the C-terminus with

truncations, deletions, chimeras and mutations. Indeed, the deletion of a single pair of aspartates within this sequence has a debilitating effect on activation by Ca^{2+} (Fig. 17A). However, without a model for the structure of this motif or for the structure that translates its binding capabilities into a mechanical force influencing channel gating, a mechanistic understanding of Ca^{2+} activation was far out of reach. There is also evidence for a second, lower affinity and less selective ion binding site (Shi et al., 2002; Xia et al., 2002). This secondary site responds to both Mg^{2+} and Ca^{2+} in the high micromolar to millimolar range. The site is independent of the primary Ca^{2+}-binding site (the Ca^{2+} bowl) and has an activating effect on channel gating over the higher range of Ca^{2+} (or Mg^{2+}) concentration. Addressing potential ion binding sites in the context of the RCK domain model, I directed a number of point mutations to the versatile binding cleft.

Recall the MthK crystal structure and the octameric ring of RCK domains with eight Ca^{2+} ions bound, one per domain. The ions are bound by a collection of residues positioned along the C-terminal ends of βA-βE, the same binding cleft shared by all similarly folded proteins. The specific residues involved in coordinating a Ca^{2+} ion are circled along the MthK sequence in the alignment in figure 10A. At analogous positions along the HBK sequence, residues targeted as potential binding residues are labeled with their corresponding number: S355, N427, Q459, Q462, and E881 (respectively in MthK: S126, D184, E210, E212, and E210). While the amino acid character of the Ca^{2+}-binding residues of MthK is not a conserved feature of RCK domains in general, the analogous positions in HBK contained some identical residues and some similar in character. At the C-terminal end of βA and βD, MthK presents a serine (S126) and an aspartic acid (D184) to participate in the binding of Ca^{2+}. The analogous positions on the first RCK domain of

HBK are S355 and N427. The mutation of S355 to alanine (S355A) has a negligible effect on function (Fig. 17B). Mutating N427 to alanine, however, results in a small but significant effect on Ca^{2+} activation, decreasing the effect of Ca^{2+}. The polar residue found in wild type perhaps makes a contribution within the binding cleft by stabilizing other charged side chains or water molecules more directly involved in ion binding.

The other major contributors to the MthK binding site are the pair of glutamic acid residues, E210 and E212. On the first RCK of HBK, there is a pair of glutamine residues in similar positions (Q459 and Q462), and on the second RCK, there is a glutamate present at position 881. The mutation of this glutamate to alanine, E881A, had a small but significant effect on Ca^{2+} activation, decreasing the effect of Ca^{2+} relative to wild type (Fig. 17B). Mutating this position to a polar glutamine, E881Q, had a larger effect in the same direction. The symmetrical positions on the first RCK domain, when mutated to glutamates, Q459E and Q462E, each had a significant effect on Ca^{2+} activation, increasing the effect of Ca^{2+}. The mutation of one of the glutamines to alanine, Q462A, had no effect at all relative to wild type. To summarize this set of mutations: the removal of a negatively charged side chain (E881Q, A) decreases the Ca^{2+} effect, while introduction of a negatively charged side chain (Q459E, Q462E) increases the effect. Despite the fact that the mutations are made in two different domains, the reciprocal effects of these reciprocal mutations is not surprising when viewed in the context of the RCK domain model. These positions are located at the C-terminal end of βE of either the first RCK (Q459 and Q462) or the second RCK (E881), and according to the structural model of domain assembly, these two regions are in close proximity to one another across the flexible interface. The effect at these βE positions however is

significantly smaller than the effect of mutating aspartates of the Ca^{2+} bowl (Fig. 17B), and they therefore may not be directly involved in mediating Ca^{2+}, instead playing an indirect role. These positions are in fact very close in the model to the primary Ca^{2+} binding site, the Ca^{2+} bowl, which itself extends from βE of the second RCK domain. Thus, the results can simply be explained as an electrostatic enhancement (or diminution) of the primary Ca^{2+}-binding site by the addition (or removal) of negatively charged residues in the vicinity of the Ca^{2+}-binding site.

Mapping the data presented here relating to potential Ca^{2+}-binding residues onto the structural model of RCK domains results in a coherent, though still speculative, functional model of Ca^{2+} activation in BK channels, consistent with the proposed model for ligand gating in MthK (Jiang et al., 2002) (Fig. 18). According to the analysis of different structures of RCK domains and RCK-like ligand-binding domains, a conformational change may involve the rearrangement of domains relative to the αF helix of the neighboring domain. Alterations at a Ca^{2+}-binding site within the adjacent clefts may then affect the conformational change. We propose that changes to the local structure and electrostatics within the binding region might induce a conformational change of the assembled domains around the hinge positions of the flexible interfaces (orange spheres in fig. 18). We now have a hypothesis for the Ca^{2+}-dependent mechanism built in to the assembled ring of RCK domains in HBK. Let us next turn to the effect of a Ca^{2+}-induced conformational change on the channel domain and on channel gating: the final step in the Ca^{2+}-activation mechanism.

CHAPTER 4

Linker Analysis

There are two general mechanisms by which one might imagine signal transduction occurring between the assembled RCK domains and the channel domain. First, the ring of RCK domains may *dock* onto the intracellular surface of the channel domain, making one or more key contacts with gating structures. Alternatively, the RCK domains may utilize the covalent link connecting them to the channel domain, directly *pulling* on the pore-forming helix. The first mechanism implies that a covalent linker is not necessary and that complementary interfaces mediate the interaction. This mechanism was tested by the co-injection of separated RCK and channel domains. Recall the dissection at site 1 from the series of co-injection tests (Fig. 13). This co-injection failed to produce currents. The result therefore suggests the importance of the covalent link between the RCK and channel domains and implies its role in the transduction mechanism.

In every case of RCK-containing K^+ channels, an RCK domain is found immediately following the last transmembrane helix. As illustrated in two crystal structures of channel domains from MthK and KcsA, the final helix is the pore-lining helix and serves as the gate of the ion conduction pathway (Jiang et al., 2002; Doyle et al., 1998). The linker, therefore, may be a crucial element in the Ca^{2+}-activation mechanism, connecting RCK domain function and channel gating. Figure 19 shows an alignment of the linker regions connecting channel domains to RCK domains. From the last conserved hydrophobic position in the final transmembrane helix to the conserved

histidine position in βA, the linkers range from 15 to 24 residues in length and consist of a high proportion of mixed charged residues indicative of a solvent exposed region. Interestingly, certain BK sequences (including HBK) maintain some of the shortest linkers among the aligned K^+ channels*. This feature is peculiar in that the linker regions and loops throughout the channels and C-terminal sequences are consistently longer in the BKs relative to the prokaryotic channels. In general, longer loops in eukaryotic sequences relative to their prokaryotic homologues are observed, suggesting the accumulation of sequence into unstructured regions, invisible to selection, over the course of evolution. The observation of a shorter linker in the BK channels, thus, suggests a purpose for this region. The nature of the role played by the linker region was probed by a series of insertions and deletions.

Insertions and deletions were made in the middle of the linker around a native GGS motif, an ideal template for a potentially unstructured, hydrophilic sequence. Figure 20A lists the specific sequence inserted and deleted relative to wild type. Insertion of residues into the linker had a significant effect on the function of HBK channels, decreasing the effect of Ca^{2+} activation. The effect was consistent at both low and high Ca^{2+} concentrations, and, to a first approximation, linear with the size of the insertion over a range of one to six residues. Comparing macrocurrent traces of wild type and the insertion of six (+6) at low and high Ca^{2+} concentrations, the insertion clearly causes a significant decrease in activation and increase in deactivation kinetics (Fig. 20B). The

* Exceptions include certain Slo2 (BK2) sequences which are longer, and the single prokaryotic sequence, Facid393_2u, which is shorter by one residue.

G-V curves at each Ca^{2+} concentration are severely right shifted for the insertion +6, relative to wild type curves (Fig. 20C). Note that the maximum open probability was not independently determined in this case and may in fact be significantly less than unity as we ran into the limit of our amplifiers at 200mV. Data from currents that do not reach a maximum open probability of unity would be artificially left-shifted by normalization to unity. Therefore, the G-V curves are not quantitative and, in this case, may underestimate the right-shifting effect. These results support a role for the linker in transducing the Ca^{2+}-induced conformational change of the RCK domains to the channel region, perhaps, for example, by physically pulling on the ends of the gating helices and thereby destabilizing the closed conformation of the channel. The destabilization might translate into an activation of the voltage-dependent process of gating. By making insertions into the linker, the amount of force pulling on the gating helices might be decreased thereby activating gating to a lesser extent. If the linker is acting as a tether in this sort of simple mechanical function it would be predicted that the insertion of some number of residues greater than six would allow enough slack in the tether that the linker would no longer transduce a force onto the gating helix and the channel would be rendered Ca^{2+} insensitive. Though we have yet to test a linker insertions greater than six, we would further predict the voltage dependence to be fairly weak with a zV_{50} greater than 200mV (the value for +6 at low Ca^{2+})*.

Deletion of residues from the wild type linker were not well tolerated, having a significant effect on the fundamental equilibrium of the channel. The deletion of a single residue (-1) caused a large shift in the behavior at low Ca^{2+}. The activation kinetics were

* The lower voltage dependence relative to other voltage-gated channels may even be indicated by the deviated S4 helix which contains significantly fewer gating charges (Diaz et al., 1998).

greatly increased, the G-V curve was left-shifted and the channels always maintained a significant open probability even at –200mV and in nM Ca^{2+}. Again, since the open probability was not quantitatively determined, the G-V analysis is not quatitative and is almost certainly biased by the normalization from zero to one due to the constitutive, non-zero open probability. A constitutive open probability is not typical of left-shifting or activating effects. With the zV_{50} at around +40mV, the channels would be expected to be fully closed at –200mV, as is demonstrated by wild type G-V curves activated by high Ca^{2+} (Fig. 20C). By deleting a single residue in the linker, we have crossed a threshold. If we again hypothesize that the linker functions as a simple tether, we can offer a possible explaination for this behavior. The deletion of one amino acid from the linker may destabilize the closed state of the channel to the point where even in the absence of Ca^{2+} the transition to the open state is on the order of kT, resulting in channel openings from background thermal energy. Deletion of two residues resulted in a significant decrease in current expression, presumably by the destabilization of the protein. Macrocurrents were observed after 11 days of incubation from an exceptionally long-lived batch of oocytes and demonstrated similar properties to the –1 currents, including a persistent open probability. We did not observe currents from the expression of a construct with three residues deleted from the linker region.

The analysis of the linker region suggests a role for the linker, potentially as a transducing element of the Ca^{2+}-activation mechanism. The results provide a possible link between the Ca^{2+}-induced conformational change of the RCK domain assembly and the gating process in the channel domain, and complete the proposed model of Ca^{2+} activation in BK channels.

CHAPTER 5

DISCUSSION

Model-Based Interpretation of Mutation Data

The utility of the RCK model is best demonstrated by providing a mechanistic interpretation to mutation data presented here and elsewhere relating to the Ca^{2+} activation of BK channels. Mapping relevant data onto the structural model elucidates the role of mutations affecting Ca^{2+} activation. Furthermore, the analysis of mutations in the context of a structural and functional model provides a means to understanding the Ca^{2+}-activation mechanism itself. The point mutation, M513I, for example, has a debilitating effect on Ca^{2+} activation (Bao et al., 2002). When combined with a mutation of Ca^{2+} bowl residues, M513I practically abolishes all high-affinity Ca^{2+} activation, rendering the channel Ca^{2+} insensitive. Due to its chemical nature, it was reasoned that M513 was probably not involved in direct coordination of Ca^{2+}, but rather involved indirectly in the Ca^{2+}-activation process. When mapped onto the RCK domain model, this residue aligns with the C-terminal end of αG of the first RCK domain in HBK (Fig. 10A). According to the model, the residue is in contact with αF of the second RCK domain and thus in structural contact with the hinge region of the flexible interface (Fig. 21). Mutating residue M513 may therefore disrupt the flexible interface and affect the conformational change responsible for transducing the Ca^{2+} effect. A similar role may be played by the deletion of loop Δ16, which immediately follows residue M513 and has an identical effect on Ca^{2+} activation. The effect at the Ca^{2+} bowl and the effect at a region

>350 residues away in a separate domain (M513) are brought to bear on the same functional element, the flexible interface, by the RCK domain model.

Another set of point mutations, D362A and D367A, were found to affect the primary Ca^{2+}-activation mechanism (Xia et al., 2002). In conjunction with Ca^{2+} bowl mutations, these point mutations also abolished Ca^{2+} activation. Independently, a similar effect was demonstrated by the mutation of an overlapping set of residues, D367-D370 (Shi et al., 2002). The analogous positions to D362 and D367 are indicated in the structural model (Fig. 21). Significantly, these positions also interact with αF of the second RCK domain across the flexible interface. Furthermore, D362 is in direct contact with the previously mentioned M513 position. Thus, the explanation for this set of mutations is the same as that for the M513 mutation: the effect is due to the disruption of the interface about which the Ca^{2+}-induced conformational change occurs. The function of these independently identified sets of mutations, distant in primary sequence from one another and from the Ca^{2+} bowl, is immediately understood when viewed in the context of the 3-dimensional structure of RCK domain assembly provided by MthK and tested in HBK

The first significant contributions to understanding the role of the Ca^{2+} bowl and surrounding C-terminal sequence were made early on in work presented in the introduction (Schreiber et al., 1999). The study of chimeric tail domains using mSlo1 and mSlo3 sequences is particularly enhanced by the presentation of a structural model. Of course at the time, the boundaries for the chimeras were chosen arbitrarily with respect to structure. The RCK domain model provides structural meaning and a new perspective from which to view the results. Recall that the combined restoration of two stretches of

mSlo1 sequence (region B and region C) into the mSlo3 tail fully restored mSlo1 Ca^{2+} activation function. Region B (881 914 in HBK) contains the Ca^{2+}-bowl sequence and a few flanking residues that are mostly redundant between the two BK variants. The significant restoration of Ca^{2+} activation by region B was therefore readily interpreted according to the ideas of Ca^{2+} bowl function. The additional restoration by region C (905 948 in HBK), however, was not interpretable. Surprisingly, even replacing region C by itself restored the same proportion of the Ca^{2+} activation as it did in combination with region B. The result directly implicated this sequence in the Ca^{2+}-activation mechanism. According to the RCK domain model, region C encompasses the major helices composing the flexible interface of the second RCK domain. There are significant sequence differences in this region between mSlo1 and mSlo3 (18 conservative and 11 non-conservative substitutions, for a total of 29 substitutions in the 45 amino acid stretch), each having evolved to function with its own unique version of the Ca^{2+} bowl region. These differences in sequence can equivalently be viewed as a set of 29 relative point mutations. Thus, having mSlo3 sequence in region C may disrupt the function of the flexible interface in a way similar to the point mutations discussed above (M513 and D362,7)(Fig. 21). Likewise, having mSlo3 sequence in region B is effectively a mutation of the Ca^{2+} bowl. Altogether, the specific residues and regions that have been found to severely affect Ca^{2+} activation are brought together by the RCK domain model and focussed on the same hyposthesized functional element, the flexible interface.

In the same study of tail chimeras (Schreiber et al., 1999), another region of sequence was found to significantly alter Ca^{2+} activation. Region A (790 880 in HBK) when restored to mSlo1 sequence, shifted the response to Ca^{2+}, decreasing the effect of

Ca^{2+} activation. The result suggested that this region was acting as an inhibitory region in wild type mSlo1. The sequence differences between mSlo1 and mSlo3 in region A include positions from βD to βE according to the RCK domain model. Significantly, interfacial positions and a salt bridging residue are effectively mutated by the swap of mSlo3 sequence in place of mSlo1 sequence (L822M, K828Q and I879L in HBK numbering). These interfacial and salt-bridging positions are uniquely conserved in RCK domains, and as demonstrated by point mutations presented here (Figs. 15 and 16), the mutation of these positions results in the disruption of Ca^{2+} activation. The effect of region A, therefore, can be explained by the mutation of crucial structural features resulting from the sequence swap.

Each of the structural interpretations discussed above naturally generates a series of hypotheses, testable by further experiments. For example, can the effects of the swaps described above be recreated with the set of point mutations predicted to bear the weight of the functional effect? The generation of new, testable hypotheses is, of course, one of the primary goals of a model. Another goal of a model is to provide an accurate picture of the actual subject in as much detail as possible. Protein crystallography has set the standard for structural models at the level of atomic resolution. High-resolution structural models then serve to produce detailed hypotheses about higher-order structure and function. Structure, however, is not function; we are still unable to determine the energetics of the protein as it breathes and as it functions from a crystal structure alone.

The model presented here is based on the structural study of prokaryotic homologs, providing the high-resolution structural information, and also on a broad series

of electrophysiological studies testing the alignment of BK domains with RCK domains and providing a glimpse of how the structure might conduct the function of Ca^{2+} activation. The functional studies focussed on features suggested by the analysis of RCK domain structures, such as the salt bridge and interfacial positions. Presumably there are additional residues throughout the protein domains that participate in the transduction process that have not been highlighted by this study. Nevertheless, our hypothetical model of Ca^{2+} activation provides the first and only model for the initial Ca^{2+}-binding event, the transduction of the binding energy into a large conformational change involving multiple structural features covering both RCK domains, and the transduction of the domain movement to the channel domain through a linker sequence. We have presented a hypothesis for the detailed structure and function of the C-terminal domains in a model of Ca^{2+} activation in BK channels.

Differences Between HBK, MthK, and Other Prokaryotic K^+ Channels

One clear difference among RCK domains is the nature of their ligand. The Ca^{2+} binding residues observed in MthK are not conserved in other prokaryotic examples. Instead, the majority of RCK domains from prokaryotic K^+ channels and transporters maintain an NAD(+)-binding motif. The function of this sequence motif was confirmed by the co-crystallization of NAD(+) with an RCK domain (Roosild et al., 2002). Then there are the remaining examples of prokaryotic RCK domains for which we have neither evidence nor indication of a specific ligand (e.g., *E. coli* kch). The eukaryotic BK family of channels has a unique ligand-binding region (the Ca^{2+} bowl) in one of the two RCK domains encoded in each of its members. Nothing resembling a Ca^{2+}-bowl region is

found in any of the prokaryotic sequences. One thing all of the ligand binding regions do have in common, however, is their placement with respect to the fold topology: they are all in the binding cleft. Furthermore, additional residues within the binding cleft of HBK RCKs were found to be analogous to the ligand-binding residues of MthK in the correlation of sidechain charge and Ca^{2+}-binding activity (Fig. 17).

In BK channels, a second Ca^{2+}-binding site was suggested by the extended response to Ca^{2+} (and Mg^{2+}) into the millimolar range (Golowasch et al., 1986; Shi and Cui, 2001; Zhang et al., 2001). Two labs independently concluded that this secondary binding site is located at the N-terminal end of βC (Shi et al., 2002; Xia et al., 2002). Like the Ca^{2+} bowl, this secondary Ca^{2+}-binding site also appears to be unique to BK family sequences as it is not conserved in prokaryotic sequences.

Another significant region of variation among RCK domains is in the C-terminal half of the domain, the subdomain which follows αG (βG-αJ in MthK). This region is in fact completely missing in a few examples of prokaryotic RCK domains, primarily those containing six transmembrane domains like *E. coli* kch that terminates at αG (refer to Appendix B). In general the sequence within this subdomain is less well conserved making the alignment ambiguous for particular sequences at certain positions within the region. The most dramatic example of deviated subdomain sequence is in the second RCK domain of BK channels. The strongest indication for the alignment is the conservation of the final beta strand where the structural terminus of the model correlates with the functional terminus of the HBK protein as determined by deletions and truncations (recall Δ58). However, regions between βE and this final beta strand may not be accurately aligned. As suggested by the failed loop deletion, Δ34, the subdomain of

the second RCK may not even be accurately modeled, having regions of conservation not accounted for by the RCK domain model. An alternative model based on a serine protease structure has been proposed for this region (Moss et al., 1996a). However, the protease model extends beyond the subdomain and clashes with the RCK domain model in key regions including the Ca^{2+} bowl and flexible interface and is therefore inconsistent with the model presented here. The low sequence conservation and, in some cases, absence of the subdomain suggests a small to negligible role in RCK domain structure and function. The model presented here places very few constraints on this region. Removing or altering the subdomain would not change the key features of RCK domains. The ligand-binding and salt-bridging residues of the domain would be maintained, as well as the major domain interfaces. This was demonstrated in the characterization and crystallization of truncated KtrA domains (Roosild et al., 2002). According to the RCK domain model presented here, only one interfacial element would be missing, the second beta sheet (red) which interfaces with the outer face of αG (see Fig. 10A). Thus, it is conceivable to maintain the overall function of RCK domains with the dramatic variation seen in the aligned subdomains.

Differences Between HBK and Other Eukaryotic BK Channels

The family of BK channels consists of three main groups, Slo1, Slo2 and Slo3, each with uniquely conserved sequence and function. Despite the diversity, all BK channels maintain the same sequence features that define the structure, assembly and function of RCK domains. The similarity in structure and basic mode of function is demonstrated by the successful domain swaps between orthologs (mouse and *Drosophila*

Slo1) and between paralogs (mSlo1 and mSlo3), and by the heterotetramerization of Slo1 and Slo2 (Wei et al., 1994; Schreiber et al., 1999; Moss and Magleby, 2001; Joiner et al., 1998). The most conspicuous regions of sequence divergence identifying these separate groups of BK channels are the Ca^{2+} bowl and certain loop regions.

Interestingly, the divergence of the Ca^{2+}-bowl region among the BK variants correlates with ligand sensitivity. While the string of aspartates in the Slo1 members (i.e., DQDDDDDPD) provides for the high-affinity Ca^{2+} binding (Schreiber and Salkoff, 1997), the Slo2 and Slo3 members make use of alternative sequences. In Slo2 channels most of the aspartates of the Ca^{2+} bowl are replaced with positively charged residues (e.g., KKERKRGSH) and the channels are activated by both Cl^- and either Ca^{2+} or Na^+ (Yuan et al., 2000; Yuan et al., 2003). In Slo3 members the sequence is mostly neutral (e.g., EQMGGLDGMLKG) and the channels are no longer activated by Ca^{2+}, but instead are pH sensitive (Schreiber et al., 1998). The variety of ligand-binding sites observed in these BK examples demonstrates the classic versatility of the binding cleft, using the variable loop regions extending from the ends of a well-defined beta sheet to define variable specificity in the context of a stable structural scaffold. The flexibility of the fold topology allows for the variable activation of the same functional mode of RCK domains. Given that each of these variant binding loops co-evolved to work with the adjacent flexible interface, each type of RCK domain could maintain the transduction of binding into a conformational change.

The loop regions, as defined by the RCK domain model, vary considerably among the BK family members. Some loops are found only in Slo1 (BK) and Slo3 (BK3) sequences and not in Slo2 (BK2); while others are exclusively found in Slo2 (refer to

Appendix A). In the loops that are shared, there is little to no sequence similarity across the different members. While loop regions are extraneous with respect to the RCK domain model and are even removable in some cases, they may play a role unique to the BK family. For example, certain loops may provide interfaces or substrates for particular accessory proteins known to associate with the C-terminal domains of BK channels (Kinases (Wang et al., 1999; Alioua et al., 1998; Alioua et al., 1998); Slob (Schopperle et al., 1998); Slip (Xia et al., 1998); BPTI (Moss et al., 1996b)). Another source of loop variation among BK channels is alternative splicing. While some splice variants consist of only conservative amino acid changes, others contain significant insertions into loop regions. The variant sequence can modulate the functional properties of the channel (Lagrutta et al., 1994; Rosenblatt et al., 1997; Liu et al., 2002). The tuning of BK channel function and the interactions with accessory proteins and their intracellular signaling pathways are critical to the many physiological roles played by BK channels.

Understanding BK Channel Function and Beyond

The structure-based analysis of the sequence, assembly and function of the C-terminal domains of BK has provided a model for Ca^{2+} activation in this important class of channels. The proposed model is a mechanistic description of a process involving binding events, protein conformational changes, and mechanical pulling forces, implying the transduction of energy through protein structure. With the high-resolution structural information from prokaryotic homologs, the model is rich in detail, highly constrained and therefore highly testable. The experiments presented here support the model and demonstrate its utility as a framework for designing and interpreting future experiments.

Beyond the study of the isolated function of BK channels, the RCK domain model will further serve investigations into the role played by BK channels at the cellular level. BK channels are involved in numerous signaling pathways. Not surprisingly, the most intensely studied pathways related to BK channel function involve Ca^{2+} signaling. In addition to the examples mentioned earlier of presynaptic and cochlear function, BK channels are important targets for controlling Ca^{2+} levels during ischemic stroke and seizures, and for controlling corporal smooth muscle (Gribkoff et al., 2001; Jin et al., 2000; Sztriha et al., 1985; Christ et al., 1998). The intracellular domains of BK channels, however, are more than Ca^{2+} sensors. There is a growing list of interesting proteins that directly interface and react with BK channels. These interactions can be studied in greater detail with the structural model provided by RCK domains. The model may further provide insight into the functional relevance of the interactions with respect to BK channels. These are the first steps to ultimately understanding how BK channels integrate and interact within the web of signaling that takes place in the living cell.

MATERIALS & METHODS

Sequence Alignment and Analysis

Multiple sequence alignments were built from sequences retrieved from non-redundant, microbial, and unfinished genomic databases (NCBI, Sanger, JGI, UOKNOR, TIGR*) using Ψ-Blast and manual iterations of Blast (Altschul et al., 1997). Queries used in the search of BK-related sequences included representative full-length BK sequences. Sequence identifications are provided in Appendix A. The collection of RCK domain sequences involved a variety of queries, including (1) full-length channel sequences with associated RCK domains, (2) stretches of sequence starting from the K+ channel signature sequence through to the initial region of an associated RCK domain, and (3) RCK domain sequences alone. Sequence identifications are given in Appendix B. ClustalW (BCM) was used to align similar segments of closely related sequences. The manual alignment of more distantly related sequences included information from (1) the Blast output, (2) structure-based similarity groups, (3) structural information from the crystal structures of RCK domains and other unrelated proteins with α-β-α layered topologies, and (4) the pattern recognition capabilities of the human visual system. Sequence similarity groups used in the determination of conservation patterns are based on chemical and structural consideration: 1. DE (negative), 2.KR (positive), 3.GP (structural), 4.ACFILMTVWY (hydrophobics composing the core of RCK and other α-β-α layered proteins).

* Preliminary sequence data were obtained from The Institute for Genomic Research website at http://www.tigr.org.

Construct Design and Mutagenesis

Our wild type human BK gene, HsloM3 (here referred to as the HBK gene), was generously provided by Ligia Toro in a pcDNA3 vector and served as the template for further subcloning and mutagenesis. A modular approach to construct design was employed using NheI restriction enzyme recognition sites. Pairs of NheI sites were used in the cloning of various segments of the HBK gene into vectors for protein expression in bacteria and in SF9 cells via a baculoviral system. The use of a single recognition site allowed for efficient modularity and swapping of N-terminal and C-terminal functionality. The same pairs of NheI sites were also used to modify the gene within the pcDNA3 vector for expression of constructs in oocytes identical to the constructs expressed for biochemical quantities of protein. Pairs of NheI sites could also be used to make truncations and deletions. Truncations were made by cutting out the intervening sequence between an NheI site at an end of the gene and a second site within the gene and ligating the resulting vector-containing fragment with itself. A large number of truncations and complementary pairs of constructs were efficiently constructed utilizing templates with an NheI site either at the start of the gene (for N-terminal truncation) or at the end (for C-terminal truncation). Likewise, significant deletions within the gene were made with pairs of NheI sites defining the boundaries of the segment to be deleted. NheI recognition sites (GCTAGC) were used in frame with the gene and thus encoded a pair of residues (ALA, SER) that resulted in the mutation of some positions at the boundaries of constructs. The general N-terminal NheI site replaced the third and fourth positions, mutating the sequence from A,L to A,S. The general C-terminal NheI site is positioned outside of the coding region between two stop codons (TGA), an upstream stop encoded

in the original plasmid and an engineered downstream stop to serve in C-terminal truncations.

Site-directed mutagenesis of the HBK gene was performed using the Quick Change (Stratagene) strategy, where a complementary pair of primers encoding the mutation are extended around the entire plasmid (9653bp) using high-fidelity Pfu Turbo polymerase to produce amplified quantities of complete, viable plasmids carrying the mutagenized gene. This approach was used in making point mutations, recognition sites, insertions of 3-18 bases and deletions of 3-102 bases. Insertions larger than 18 bases were difficult to encode in mutagenesis primers and were thus performed by cutting and pasting cassettes of sequence defined by NheI sites, or by designing oligos to directly serve as the double-stranded insert. While deletions of up to ~50 bases were readily obtained using a pair mutagenesis primers, attempts at larger deletions (>100 bases) failed, with one exception of 102 bases in the construction of Δ34. Deletions greater than 102 bases were performed by using pairs of NheI sites as described above.

Protein Expression and Purification

Bacterial

Segments of the HBK gene were subcloned into pET28b(+) for heterologous expression in *E. coli* BL21(DE3). The transformed *E. coli* cells were grown in LB medium at 37°C and protein expression was induced with 0.4-1.0mM IPTG at either 37°C for 1-3 hours or 22°C overnight. Soluble protein was extracted from lysed cell harvests with 20mM Tris-HCl pH 7.5 and a range of salt concentrations (200mM NaCl, 500mM NaCl, or 1M KCl). Additional solubilization attempts were made with low pH

buffer (Na-acetate), lower temperature preparations, and the addition of reducing agent (DTT), 1mM $CaCl_2$ and below CMC quantities of mild detergents (e.g., β-octoglucoside).

Protein derived from construct G was successfully extracted in a buffer containing 20mM Tris-HCl pH 7.5, 200mM NaCl, 1mM DTT, and 1mM$CaCl_2$ at 4°C and purified on a Talon Co^{2+} affinity column via an engineered N-terminal 6xHIS tag. Following elution with 200mM Immidazole, the HIS tag was cleaved by Thrombin. With a pI of 4.6, protein G was further purified on a MonoQ column with a linear salt gradient from 200mM to 1M NaCl, eluting near 400mM NaCl. A final gel filtration step (Superdex-200) allowed for characterization and purification by size (or, more precisely, the effective radius of the globular protein or protein complex) and the exchange into buffer containing 10mM Tris-HCl 7.5 and 1mM $CaCl_2$ for crystallization trials, extensively screened at 20°C and at 4°C.

Baculoviral

Segments of the HBK gene were subcloned into a modified pAcG2T vector with an NheI site (bold) inserted between BamHI and EcoRI sites (underlined) of the original multiple cloning region: GGATCC**GCTAGC**GGAATTC. The vector contains an N-terminal glutathione-S-transferase (GST) tag and thrombin cleavage site. Co-transfection and recombination with viral DNA into cultured SF9 insect cells yields baculoviral protein expression. Baculoviral DNA is amplified to increase infection titer through rounds of SF9 cell infection and collection of the enhanced, virus-containing media. Liters of suspended SF9 cells were infected with high-titer baculoviral DNA. Protein expression peaked approximately 4 days following infection. Soluble protein was

extracted from lysed SF9 cell harvests with 50mM Tris-HCl pH 7.5-8.0, 150mM NaCl and 1mM $CaCl_2$. The GST-tagged protein was bound to a glutathione-sepharose column and washed with the same buffer at a lower concentration of Tris (20mM). The GST tag was cleaved from the protein while still bound to the column by the addition of Thrombin, and the protein was simply rinsed off the column. The protein was further purified on a MonoQ column with a 150mM NaCl wash and 400mM NaCl elution. A final step of gel filtration allowed for characterization and purification of the protein by size. Gel filtration buffers contained 20mM Tris-HCl pH 7.5-8.0 and 150mM NaCl with the addition of either 10mM DTT, 2mM EGTA or 1mM $CaCl_2$. Following gel filtration, the protein was concentrated to 5-10mg/mL and used to screen crystallization conditions.

Channel Expression in Oocytes

Full length, truncation, deletion, and mutation constructs of the HBK gene were transcribed, *in vitro*, into RNA for injection into *Xenopus leavis* oocytes. T7 RNA transcription was initiated by an hCMV promoter within the original pcDNA3 vector which also contained a ribosome binding site, 5' UTR from Shaker, 3' UTR from hSlo1(M3), poly-A tail, and NotI restriction enzyme recognition site for linearization. RNAs were purified by Trizol method (Gibco-BRL) or RNeasy kit (Qiagen) and stored at -80°C. Oocytes were dissected from anesthetized *Xenopus leavis* (African clawed frogs) by a survival surgery. Oocytes were immediately treated with collagenase (2mg/mL) for 1.5 hours, rinsed with a Ca^{2+}-free OR-2 solution (in mM: 82.5 NaCl, 2.5 KCl, 1 $MgCl_2$, 5 Hepes-NaOH pH 7.6) and stored in ND-96 solution (in mM: 96 NaCl, 2 KCl, 1.8 $CaCl_2$, 1 $MgCl_2$, 5 Hepes-NaOH pH 7.6) containing fresh gentamycin (50mg/L). Within 2 days

of dissection, oocytes were injected with 50-70nL of purified RNAs at full strength or diluted 2-5 fold. Typically, 1-3 days of incubation provided significant macrocurrents measured in patch-clamp recording.

Electrophysiology

Patch pipettes were pulled from glass capillary tubing (Warner G85150T-4) on a programmable Flaming/Brown type puller (Sutter P-97) and fire polished on a microforge using the resistive heat from a platinum wire. Polished pipettes were approximately 2μm in diameter and produced resistances ranging 0.9-2.5 MΩ in series with recording equipment. Axopatch amplifiers (Axon Instruments 200A and 200B), a low-pass Bessel filter (Frequency devices 902), a digitizer (Axon Instruments DigiData 1200A) and pClamp8.0 software (Axon Instruments) were used in the recording of data. Patch pipettes were applied to the surface of freshly devitellinized oocytes to form tight electrical seals (>10GΩ), allowing a voltage-clamp on patches of plasma membrane. Patches were excised in an inside-out configuration, exposing the intracellular face of membrane and embedded channels to a bath solution controlled by a gravity-flow perfusion system. Two stock solutions were made to control the preparation of precise, μM-range, Ca^{2+}-buffered bath solutions: a solution without Ca^{2+} (0-Ca), containing (in mM) 130 Kgluconate (Fluka), 20 KCl (Fluka or Fisher), 20 Hepes-KOH pH 7.5 (Fisher), and 5 EGTA (Fisher); and a 1000μM free-Ca^{2+} solution (1000-Ca) containing an additional 6 $CaCl_2$ (Fluka) buffered by the EGTA. A series of Ca^{2+}-buffered solutions ranging from 1μM to 300μM free Ca^{2+} were then made by mixing together quantities of 0-Ca and 1000-Ca based on an EGTA-Ca^{2+} K_d of $3.86*10^{-7}$. The pipette solution was

prepared by the addition of 2 $MgCl_2$ to a 1-3μM Ca^{2+}-buffered solution. To control solution-dependent variables, reference recordings of wild type HBK channels were made for each batch of solutions in order to verify the range of Ca^{2+} concentrations and to serve as a specific control for the data collected using those solutions. In addition, reference wild type injections and recordings were made to control variables dependent on oocyte batches, RNA preparations, seasons of the year, etc. Material and temporal variables were controlled for each study involving the comparison of wild type and mutant data.

Patches were voltage-clamped at 0mV between recordings for stability. A typical episodic voltage protocol consisted of 2-3 averaged runs of 16 sweeps stepping from a holding potential of 0mV to a range of test voltages in 20mV steps for 30ms, activating channel currents, and then stepping to tail voltage of -60mV for 10ms to produce tail currents. Current signal was filtered at 4kHz (-3dB), digitized at 20kHz, and recorded onto hard disk. Records were processed and parameterized using Clampfit (Axon Instruments), Origin (Microcal Software), and Excel (Microsoft) programs. Data points were extracted from the tail currents 200μs following the tail voltage step in order to determine the voltage dependence. Fit with the following equation,

$$G = G_{max}/(1 + \exp(-(V-V_{50})zF/RT)) + AV + B$$

where G is the conductance measured as tail current divided by tail voltage and V is the applied test voltage, the data are described by a Boltzmann function (to account for the transition of a population of channels from closed to open states) summed with a linear function (to account for leak current) and normalized by G_{max} (the maximum value of G obtained in the data set). The terms of the Boltzmann equation include z as the gating

charge, V_{50} as the voltage at which 50% of the channels are open, and F, R and T which have there usual meaning. The linear equation includes terms A and B to represent the slope and y-intercept, respectively. A thorough study of macroscopic BK currents and current analysis serves as the basis for methodology used here (Cox et al., 1997a; Cox et al., 1997b).

REFERENCES

Adelman,J.P., Shen,K.Z., Kavanaugh,M.P., Warren,R.A., Wu,Y.N., Lagrutta,A., Bond,C.T., and North,R.A. (1992). Calcium-activated potassium channels expressed from cloned complementary DNAs. Neuron *9*, 209-216.

Alioua,A., Tanaka,Y., Wallner,M., Hofmann,F., Ruth,P., Meera,P., and Toro,L. (1998). The large conductance, voltage-dependent, and calcium-sensitive K+ channel, Hslo, is a target of cGMP-dependent protein kinase phosphorylation in vivo. J. Biol. Chem. *273*, 32950-32956.

Altschul,S.F., Madden,T.L., Schaffer,A.A., Zhang,J., Zhang,Z., Miller,W., and Lipman,D.J. (1997). Gapped BLAST and PSI-BLAST: a new generation of protein database search programs. Nucleic Acids Res. *25*, 3389-3402.

Atkinson,N.S., Robertson,G.A., and Ganetzky,B. (1991). A component of calcium-activated potassium channels encoded by the Drosophila slo locus. Science *253*, 551-555.

Bao,L., Rapin,A.M., Holmstrand,E.C., and Cox,D.H. (2002). Elimination of the BK(Ca) channel's high-affinity Ca(2+) sensitivity. J. Gen. Physiol *120*, 173-189.

Bian,S., Favre,I., and Moczydlowski,E. (2001). Ca2+-binding activity of a COOH-terminal fragment of the Drosophila BK channel involved in Ca2+-dependent activation. Proc. Natl. Acad. Sci. U. S. A *98*, 4776-4781.

Christ,G.J., Rehman,J., Day,N., Salkoff,L., Valcic,M., Melman,A., and Geliebter,J. (1998). Intracorporal injection of hSlo cDNA in rats produces physiologically relevant alterations in penile function. Am. J. Physiol *275*, H600-H608.

Cox,D.H., Cui,J., and Aldrich,R.W. (1997a). Allosteric gating of a large conductance Ca-activated K+ channel. J. Gen. Physiol *110*, 257-281.

Cox,D.H., Cui,J., and Aldrich,R.W. (1997b). Separation of gating properties from permeation and block in mslo large conductance Ca-activated K+ channels. J. Gen. Physiol *109*, 633-646.

Cui,J. and Aldrich,R.W. (2000). Allosteric linkage between voltage and Ca(2+)-dependent activation of BK-type mslo1 K(+) channels. Biochemistry *39*, 15612-15619.

Derst,C. and Karschin,A. (1998). Evolutionary link between prokaryotic and eukaryotic K+ channels. J. Exp. Biol. *201 (Pt 20)*, 2791-2799.

Diaz,L., Meera,P., Amigo,J., Stefani,E., Alvarez,O., Toro,L., and Latorre,R. (1998). Role of the S4 segment in a voltage-dependent calcium-sensitive potassium (hSlo) channel. J. Biol. Chem. *273*, 32430-32436.

Doyle,D.A., Morais,C.J., Pfuetzner,R.A., Kuo,A., Gulbis,J.M., Cohen,S.L., Chait,B.T., and MacKinnon,R. (1998). The structure of the potassium channel: molecular basis of K+ conduction and selectivity. Science *280*, 69-77.

Durell,S.R., Hao,Y., Nakamura,T., Bakker,E.P., and Guy,H.R. (1999). Evolutionary relationship between K(+) channels and symporters. Biophys. J. *77*, 775-788.

Golowasch,J., Kirkwood,A., and Miller,C. (1986). Allosteric effects of Mg2+ on the gating of Ca2+-activated K+ channels from mammalian skeletal muscle. J. Exp. Biol. *124*, 5-13.

Gribkoff,V.K., Starrett,J.E., Jr., Dworetzky,S.I., Hewawasam,P., Boissard,C.G., Cook,D.A., Frantz,S.W., Heman,K., Hibbard,J.R., Huston,K., Johnson,G., Krishnan,B.S., Kinney,G.G., Lombardo,L.A., Meanwell,N.A., Molinoff,P.B., Myers,R.A., Moon,S.L., Ortiz,A., Pajor,L., Pieschl,R.L., Post-Munson,D.J., Signor,L.J., Srinivas,N., Taber,M.T., Thalody,G., Trojnacki,J.T., Wiener,H., Yeleswaram,K., and Yeola,S.W. (2001). Targeting acute ischemic stroke with a calcium-sensitive opener of maxi- K potassium channels. Nat. Med. *7*, 471-477.

Horrigan,F.T. and Aldrich,R.W. (2002). Coupling between voltage sensor activation, Ca2+ binding and channel opening in large conductance (BK) potassium channels. J. Gen. Physiol *120*, 267-305.

Jiang,Y., Lee,A., Chen,J., Cadene,M., Chait,B.T., and MacKinnon,R. (2002). Crystal structure and mechanism of a calcium-gated potassium channel. Nature *417*, 515-522.

Jiang,Y., Pico,A., Cadene,M., Chait,B.T., and MacKinnon,R. (2001). Structure of the RCK domain from the E. coli K+ channel and demonstration of its presence in the human BK channel. Neuron *29*, 593-601.

Jin,W., Sugaya,A., Tsuda,T., Ohguchi,H., and Sugaya,E. (2000). Relationship between large conductance calcium-activated potassium channel and bursting activity. Brain Res. *860*, 21-28.

Joiner,W.J., Tang,M.D., Wang,L.Y., Dworetzky,S.I., Boissard,C.G., Gan,L., Gribkoff,V.K., and Kaczmarek,L.K. (1998). Formation of intermediate-conductance calcium-activated potassium channels by interaction of Slack and Slo subunits. Nat. Neurosci. *1*, 462-469.

Lagrutta,A., Shen,K.Z., North,R.A., and Adelman,J.P. (1994). Functional differences among alternatively spliced variants of Slowpoke, a Drosophila calcium-activated potassium channel. J. Biol. Chem. *269*, 20347-20351.

Lingle,C.J. (2002). Setting the stage for molecular dissection of the regulatory components of BK channels. J. Gen. Physiol *120*, 261-265.

Liu,X., Chang,Y., Reinhart,P.H., Sontheimer,H., and Chang,Y. (2002). Cloning and characterization of glioma BK, a novel BK channel isoform highly expressed in human glioma cells. J. Neurosci. *22*, 1840-1849.

Magleby,K.L. (2003). Gating Mechanism of BK (Slo1) Channels: So Near, Yet So Far. J. Gen. Physiol *121*, 81-96.

Marrion,N.V. and Tavalin,S.J. (1998). Selective activation of Ca2+-activated K+ channels by co-localized Ca2+ channels in hippocampal neurons. Nature *395*, 900-905.

Meera,P., Wallner,M., Song,M., and Toro,L. (1997). Large conductance voltage- and calcium-dependent K+ channel, a distinct member of voltage-dependent ion channels with seven N-terminal transmembrane segments (S0-S6), an extracellular N terminus, and an intracellular (S9-S10) C terminus. Proc. Natl. Acad. Sci. U. S. A *94*, 14066-14071.

Milkman,R. (1994). An Escherichia coli homologue of eukaryotic potassium channel proteins. Proc. Natl. Acad. Sci. U. S. A *91* , 3510-3514.

Moss,B.L. and Magleby,K.L. (2001). Gating and conductance properties of BK channels are modulated by the S9-S10 tail domain of the alpha subunit. A study of mSlo1 and mSlo3 wild-type and chimeric channels. J. Gen. Physiol *118*, 711-734.

Moss,G.W., Marshall,J., and Moczydlowski,E. (1996a). Hypothesis for a serine proteinase-like domain at the COOH terminus of Slowpoke calcium-activated potassium channels. J. Gen. Physiol *108*, 473-484.

Moss,G.W., Marshall,J., Morabito,M., Howe,J.R., and Moczydlowski,E. (1996b). An evolutionarily conserved binding site for serine proteinase inhibitors in large conductance calcium-activated potassium channels. Biochemistry *35*, 16024-16035.

Pallanck,L. and Ganetzky,B. (1994). Cloning and characterization of human and mouse homologs of the Drosophila calcium-activated potassium channel gene, slowpoke. Hum. Mol. Genet. *3*, 1239-1243.

Piskorowski,R. and Aldrich,R.W. (2002). Calcium activation of BK(Ca) potassium channels lacking the calcium bowl and RCK domains. Nature *420*, 499-502.

Quirk,J.C. and Reinhart,P.H. (2001). Identification of a novel tetramerization domain in large conductance K(ca) channels. Neuron *32*, 13-23.

Ramanathan,K., Michael,T.H., Jiang,G.J., Hiel,H., and Fuchs,P.A. (1999). A molecular mechanism for electrical tuning of cochlear hair cells. Science *283*, 215-217.

Roberts,W.M., Jacobs,R.A., and Hudspeth,A.J. (1990). Colocalization of ion channels involved in frequency selectivity and synaptic transmission at presynaptic active zones of hair cells. J. Neurosci. *10*, 3664-3684.

Robitaille,R., Garcia,M.L., Kaczorowski,G.J., and Charlton,M.P. (1993). Functional colocalization of calcium and calcium-gated potassium channels in control of transmitter release. Neuron *11*, 645-655.

Roosild,T.P., Miller,S., Booth,I.R., and Choe,S. (2002). A mechanism of regulating transmembrane potassium flux through a ligand- mediated conformational switch. Cell *109*, 781-791.

Rosenblatt,K.P., Sun,Z.P., Heller,S., and Hudspeth,A.J. (1997). Distribution of Ca2+-activated K+ channel isoforms along the tonotopic gradient of the chicken's cochlea. Neuron *19*, 1061-1075.

Schopperle,W.M., Holmqvist,M.H., Zhou,Y., Wang,J., Wang,Z., Griffith,L.C., Keselman,I., Kusinitz,F., Dagan,D., and Levitan,I.B. (1998). Slob, a novel protein that interacts with the Slowpoke calcium- dependent potassium channel. Neuron *20*, 565-573.

Schreiber,M. and Salkoff,L. (1997). A novel calcium-sensing domain in the BK channel. Biophys. J. *73*, 1355-1363.

Schreiber,M., Wei,A., Yuan,A., Gaut,J., Saito,M., and Salkoff,L. (1998). Slo3, a novel pH-sensitive K+ channel from mammalian spermatocytes. J. Biol. Chem. *273*, 3509-3516.

Schreiber,M., Yuan,A., and Salkoff,L. (1999). Transplantable sites confer calcium sensitivity to BK channels. Nat. Neurosci. *2*, 416-421.

Shi,J. and Cui,J. (2001). Intracellular Mg(2+) enhances the function of BK-type Ca(2+)-activated K(+) channels. J. Gen. Physiol *118*, 589-606.

Shi,J., Krishnamoorthy,G., Yang,Y., Hu,L., Chaturvedi,N., Harilal,D., Qin,J., and Cui,J. (2002). Mechanism of magnesium activation of calcium-activated potassium channels. Nature *418*, 876-880.

Stumpe,S., Schlosser,A., Schleyer,M., and Bakker,E.P. (1996). K+ circulation across the prokaryotic cell membrane: K+-uptake systems. In Handbook of Biological Physics, W.N.Konings, H.R.Kaback, and J.S.Lolkema, eds. (New York: Elsevier Science B.V.), pp. 473-499.

Sztriha,L., Joo,F., and Szerdahelyi,P. (1985). Accumulation of calcium in the rat hippocampus during kainic acid seizures. Brain Res. *360*, 51-57.

Wang,J., Zhou,Y., Wen,H., and Levitan,I.B. (1999). Simultaneous binding of two protein kinases to a calcium-dependent potassium channel. J. Neurosci. *19*, RC4.

Wang,Z.W., Saifee,O., Nonet,M.L., and Salkoff,L. (2001). SLO-1 potassium channels control quantal content of neurotransmitter release at the C. elegans neuromuscular junction. Neuron *32*, 867-881.

Wei,A., Jegla,T., and Salkoff,L. (1996). Eight potassium channel families revealed by the C. elegans genome project. Neuropharmacology *35*, 805-829.

Wei,A., Solaro,C., Lingle,C., and Salkoff,L. (1994). Calcium sensitivity of BK-type KCa channels determined by a separable domain. Neuron *13*, 671-681.

Wood,L.S. and Vogeli,G. (1997). Mutations and deletions within the S8-S9 interdomain region abolish complementation of N- and C-terminal domains of Ca(2+)-activated K+ (BK) channels. Biochem. Biophys. Res. Commun. *240*, 623-628.

Wu,Y.C. and Fettiplace,R. (1996). A developmental model for generating frequency maps in the reptilian and avian cochleas. Biophys. J. *70*, 2557-2570.

Xia,X., Hirschberg,B., Smolik,S., Forte,M., and Adelman,J.P. (1998). dSLo interacting protein 1, a novel protein that interacts with large- conductance calcium-activated potassium channels. J. Neurosci. *18*, 2360-2369.

Xia,X.M., Zeng,X., and Lingle,C.J. (2002). Multiple regulatory sites in large-conductance calcium-activated potassium channels. Nature *418*, 880-884.

Yifrach,O. and MacKinnon,R. (2002). Energetics of pore opening in a voltage-gated K(+) channel. Cell *111*, 231-239.

Yuan,A., Dourado,M., Butler,A., Walton,N., Wei,A., and Salkoff,L. (2000). SLO-2, a K+ channel with an unusual Cl- dependence. Nat. Neurosci. *3*, 771-779.

Yuan,A., Santi,C.M., Wei,A., Wang,Z.W., Pollak,K., Nonet,M., Kaczmarek,L., Crowder,C.M., and Salkoff,L. (2003). The sodium-activated potassium channel is encoded by a member of the slo gene family. Neuron *37*, 765-773.

Zhang,X., Solaro,C.R., and Lingle,C.J. (2001). Allosteric regulation of BK channel gating by Ca(2+) and Mg(2+) through a nonselective, low affinity divalent cation site. J. Gen. Physiol *118*, 607-636.

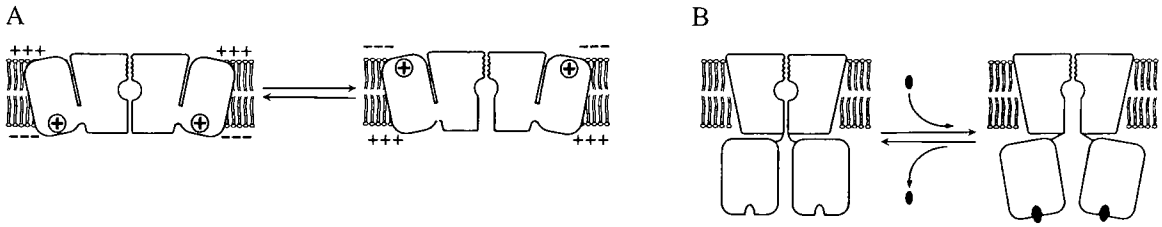

Figure 1 Voltage- and ligand-dependent gating by accessory domains of K^+ channels. (A) N-terminal voltage-sensing domains influence gating of the channel in response to changes in membrane potential. Depolarization of the membrane is associated with channel opening. (B) Ligand-binding domains, depicted as a C-terminal set of intracellular domains, can also influence channel gating. The example here shows a ligand-binding event leading to channel opening. Different ligand-binding domains confer unique ligand sensitivities to various families of K+ channels.

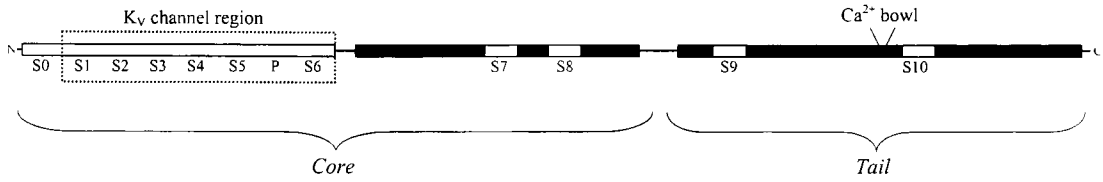

Figure 2 Linear schematic of key features noted in the initial study of BK channel protein sequences. From N-terminus to C-terminus, the ~1100 amino acid protein contains a unique S0 transmembrane helix and a well conserved S1-S6 K_v channel motif (gray) followed by a large C-terminal set of intracellular domains (black). Regions S7-S10 (gray) were initially thought to be additional transmembrane helices due to their hydrophobic sequence, but later shown to be intracellular (Meera et al., 1997). The C-terminus is divided by a variable region, defining the boundary between *core* and *tail* regions. The tail region contains the aspartate-rich sequence referred to as the Ca^{2+} bowl.

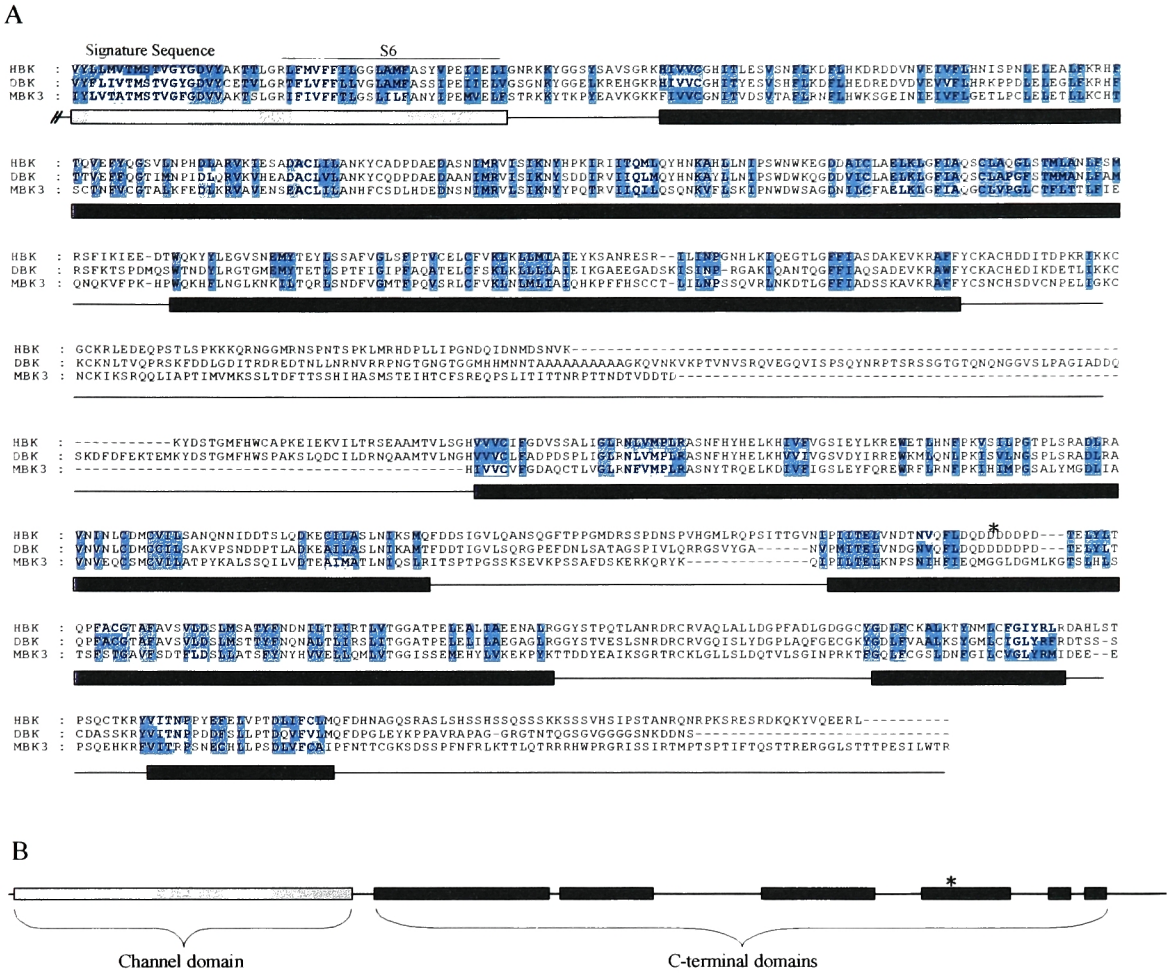

Figure 3 Representative multiple sequence alignment of BK channels and primary domain structure. (A) The conservation pattern at 80% similarity from a multiple sequence alignment of a larger set of diverse BK sequences (Appendix A) displayed on three representative sequences: HBK (human Slo1), DBK (*Drosophila* Slo1), MBK3 (mouse Slo3). The alignment begins at the K^+ channel signature sequence and ends at the C-terminus. Below the alignment, bars represent the clustering of conserved sequence as potential domains composing a primary domain model. (B) The complete primary domain model to scale with HBK sequence. The asterisk denotes the position of the Ca^{2+} bowl.

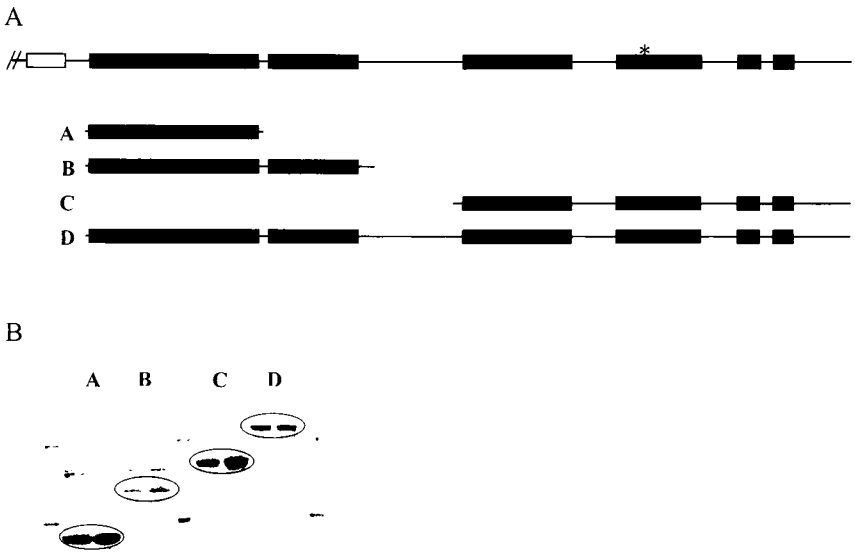

Figure 4 Expression constructs A-D. (A) Shown in schematic representation in relation to the primary domain structure (top line). (B) Insoluble fractions from pairs of expression experiments with constructs A-D were run on SDS-PAGE. Bands corresponding to proteins A-D are circled.

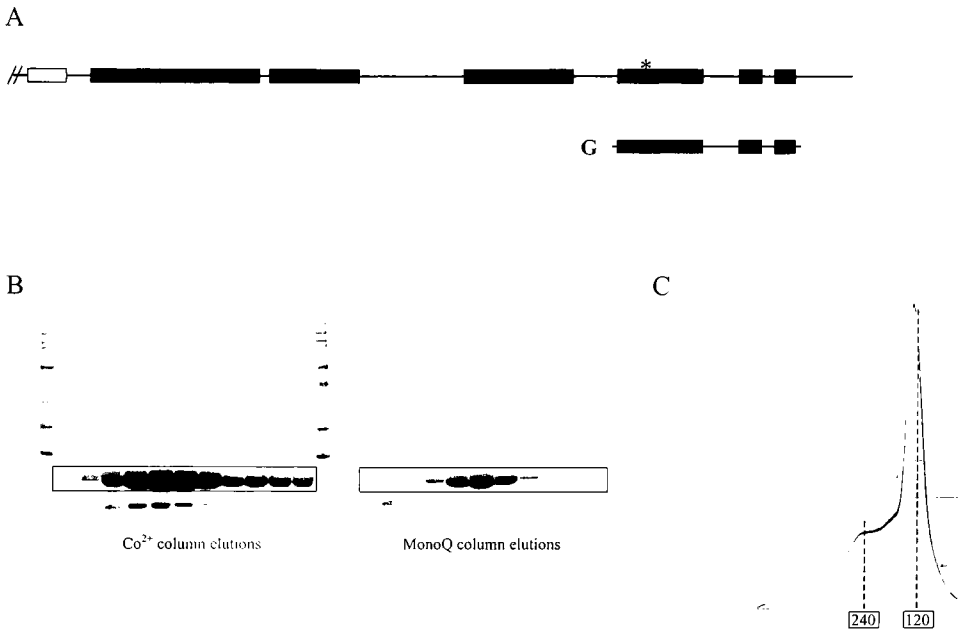

Figure 5 Purification and characterization of protein G. (A) Schematic of construct G in relation to primary domain structure. Note that the construct includes the Ca^{2+} bowl (asterisk). (B) SDS-PAGE of HIS-tagged protein G (boxed) eluted from a Co^{2+} column with 200mM Immidazole (left). Further purification of protein G by ion exchange on a monoQ column with a 0.2-1.0M NaCl gradient (right). (C) Oligameric states of purified protein G inferred from size exclusion chromatography using a superdex 200 gel filtration column. The 20kDa protein produced a major peak at ~120kDa and a large shoulder extending to ~240kDa.

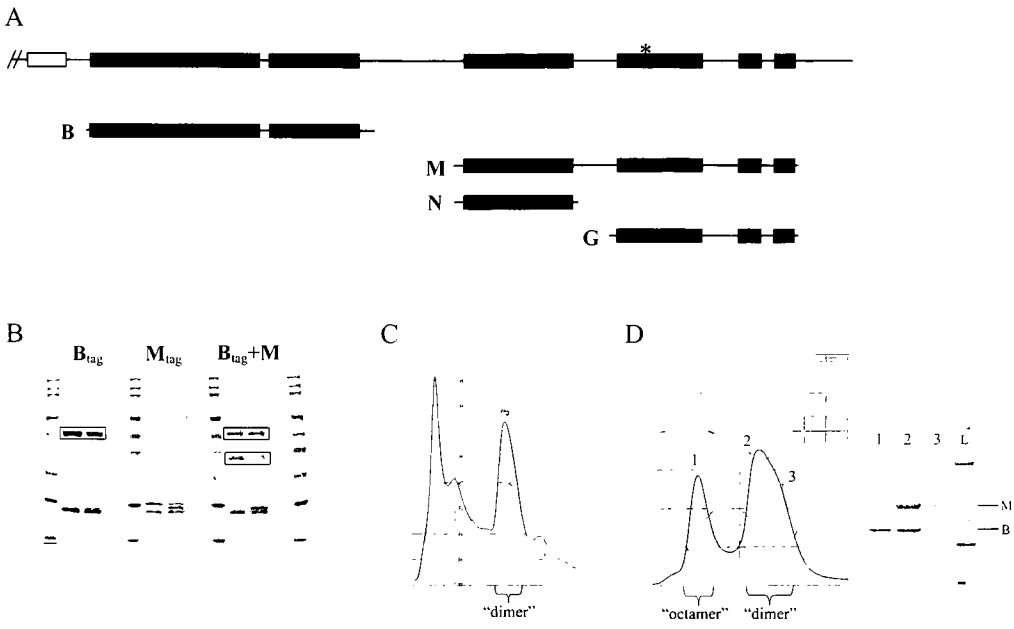

Figure 6 Co-expression in SF9 insect cells. (A) Schematics of constructs B, M, N and G in relation to primary domain structure. (B) SDS-PAGE of soluble fractions enhanced on a glutathione-sepharose column. Left lanes show GST-tagged protein B (boxed). Center lanes show the expected position of GST-tagged protein M (dashed box). Right lanes show the co-purification of GST-tagged protein B (upper box) and untagged protein M (lower box) in an approximately 1:1 ratio. (C) First run of gel filtration for B+M complex. The "dimer" peak (see text) of complex is labeled by a bracket below the chart. (D) Second run of gel filtration for B+M complex from the "dimer" peak of the first run. "Dimer" and regenerated "octamer" peaks are indicated by brackets. Numbers on peaks correspond to numbered lanes of SDS-PAGE showing proteins B and M in each region sampled during elution.

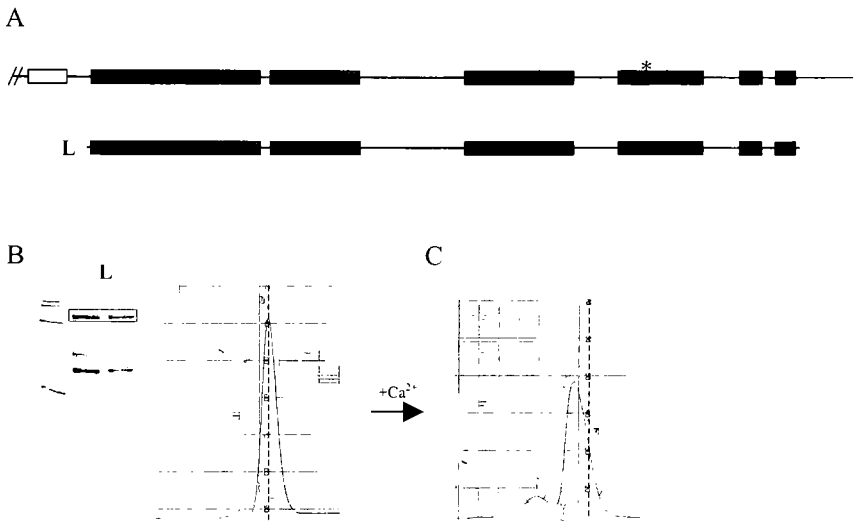

Figure 7 Characterization of protein L. (A) Schematic of construct L in relation to primary domain structure. (B) SDS-PAGE shows co-purification of full-length protein L (boxed) with a number of smaller fragments. The heterogeneous protein sample runs as a narrow peak at a mass suggesting a monomer of protein L on gel filtration. (C) In the presence of 1mM $CaCl_2$ the same protein runs at a slightly higher mass (compare to previous position: dashed line) and a new, even higher mass peak develops, suggesting an oligamer.

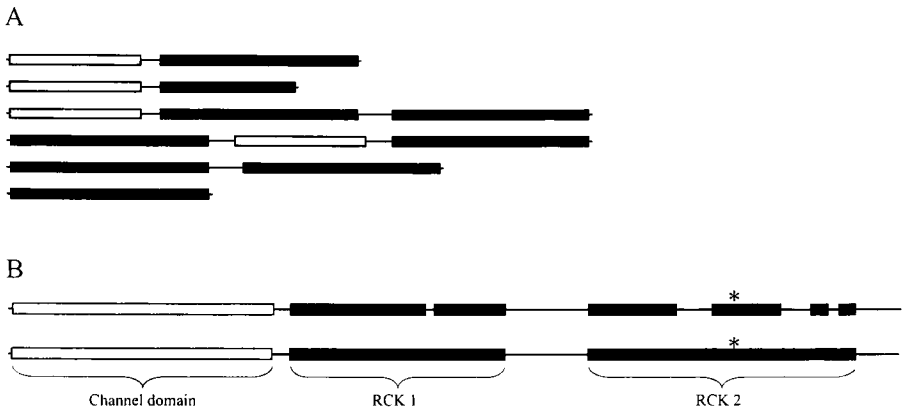

Figure 8 Different topological arrangements of RCK domains. (A) Relative positions of K^+ channel domains (gray) and RCK domains (black) as observed in identified sequences. (From top to bottom) RCK domains are found C-terminal, truncated, in tandem, at both N- and C-termini, and isolated in pairs and alone. (B) A tandem C-terminal arrangement of RCK domains is found in eukaryotic BK channels. The correspondence between the primary domain model (top), based on BK sequence analysis, and the RCK domain model (bottom) is shown by the adjacent schematics scaled with the primary sequence of HBK. The asterisk denotes the position of the Ca^{2+} bowl in each model.

A

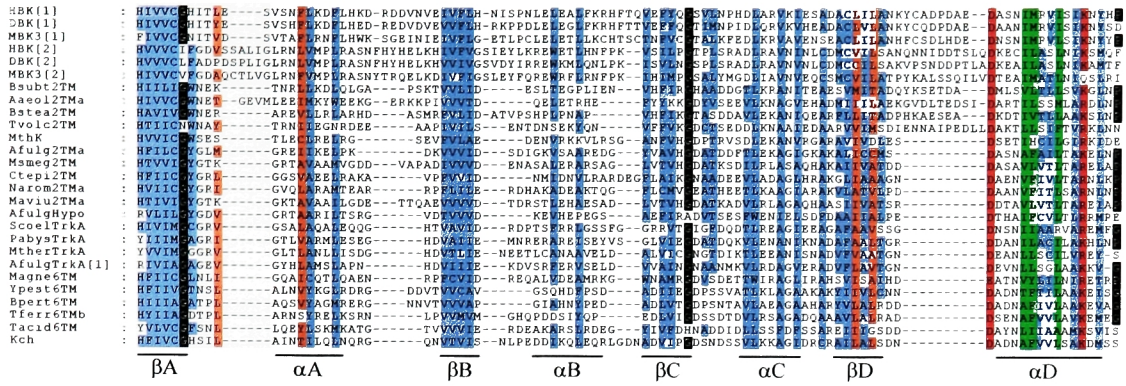

B

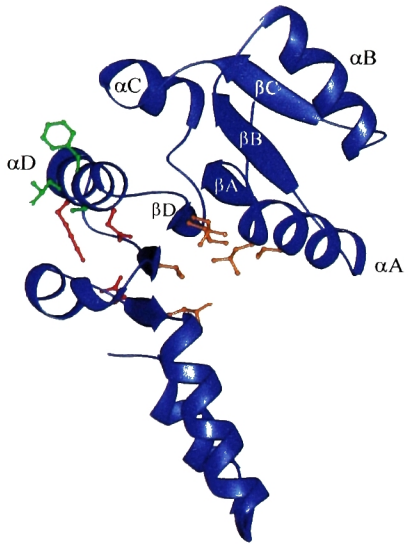

Figure 9 Multiple sequence alignment and RCK structure from *E. coli* kch. (A) A subset of RCK domain sequences aligned with the kch RCK domain (last line) from βA to αD (see Appendix B for complete alignment and sequence identities). Corresponding secondary structure is indicated below the alignment. The conservation pattern at 65% similarity is shown in light blue for this subset of sequences. Uniquely conserved positions are highlighted by color: structural GLY and PRO positions in black, interfacial positions in orange and green, and salt bridging residues in red. The orange interfacial residues complement an αF helix from a neighboring domain, and the green residues on αD interface with the analogous residues of a neighboring domain (not shown). (B) Ribbons diagram of kch RCK monomer. Secondary structure labels and color-coded side chains correspond to those of the alignment above. Note D322 of kch forms a salt bridge with a backbone amide at the C-terminal end of βE, and K333 of kch forms a salt bridge with D360 at the N-terminal end of βF.

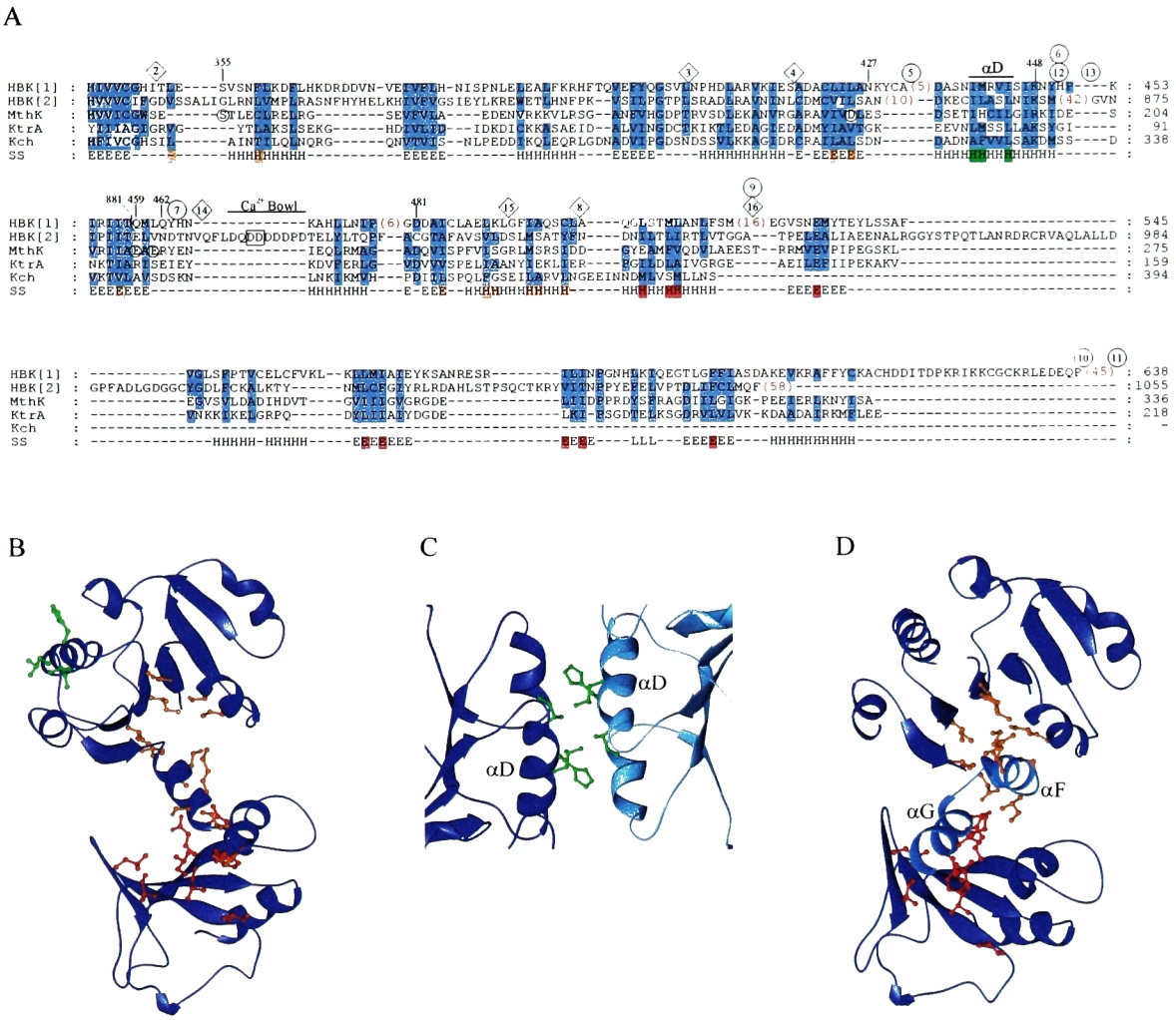

Figure 10 Representative multiple sequence alignment of RCK domains and structural relevance of conserved positions. (A) The conservation pattern at 65% similarity from a multiple sequence alignment of all available RCK domain sequences (Appendix B) displayed on representative sequences: HBK[1] (RCK1 of human BK), HBK[2] (RCK2 of human BK), MthK (PDB ID: 1LNQ), KtrA (1LSS), and Kch (1ID1). The last line (SS) indicates the corresponding secondary structure of the MthK sequence. Red numbers in parentheses relate to the results of loop deletion experiments. Numbers in circles and diamonds relate the results of co-injection experiments. Other labeled residues and regions indicate targets of a series of point mutations. Interfacial positions are highlighted in orange, green and red along the SS line. The color-coding is maintained in the ball and stick representation of interfacial positions in the context of the 3-D structure provided by MthK (B-D). (B) Interfacial positions on a single monomer. (C) The *fixed* interface between αD helices of neighboring domains distinguished by shades of blue. (D) Half of the *flexible* interface. The αF-αG interfacial element from one domain (light blue) packs against the two major beta sheets of the neighboring domain (dark blue).

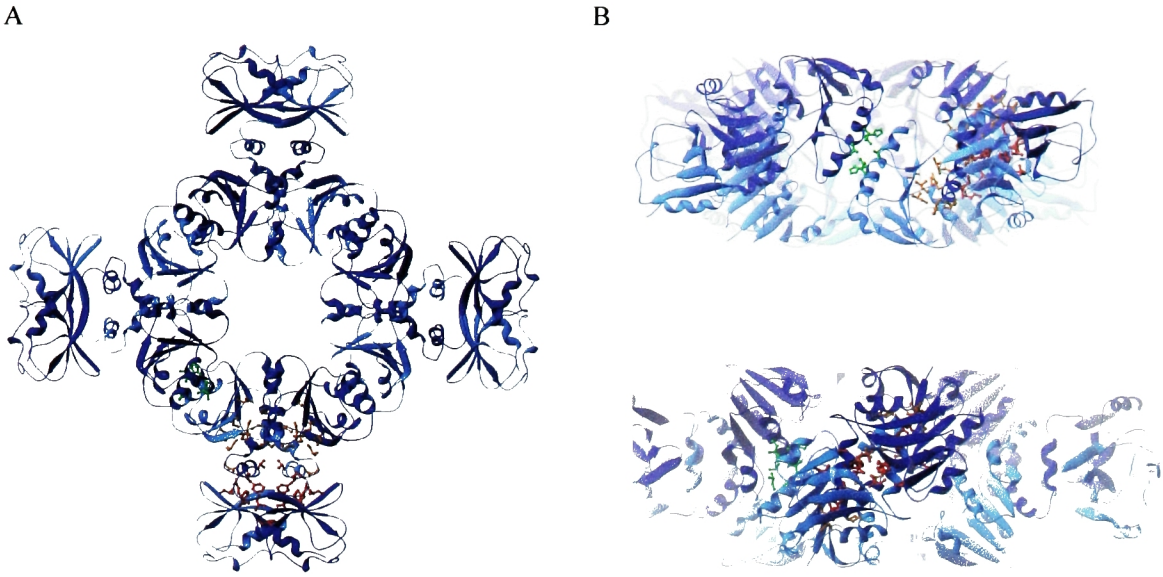

Figure 11 The full assembly of RCK domains of MthK. (A) The octameric ring from a top-down perspective with respect to the pore of the associated channel (not shown), perpendicular to the plane of the membrane. The fixed and flexible interfaces (indicated by the color coded residues) bring alternating pairs of RCK domains together to form the ring. (B) Side views (parallel with the plane of the membrane) focussing on the interfaces separated by a 45° rotation: the fixed interface (top) involving two αD helices, and the flexible interface (bottom) involving the swap of αF-αG elements. Notice the light-blue helices interfacing with the dark-blue beta sheets, and the dark-blue helices interfacing with the light-blue beta sheets.

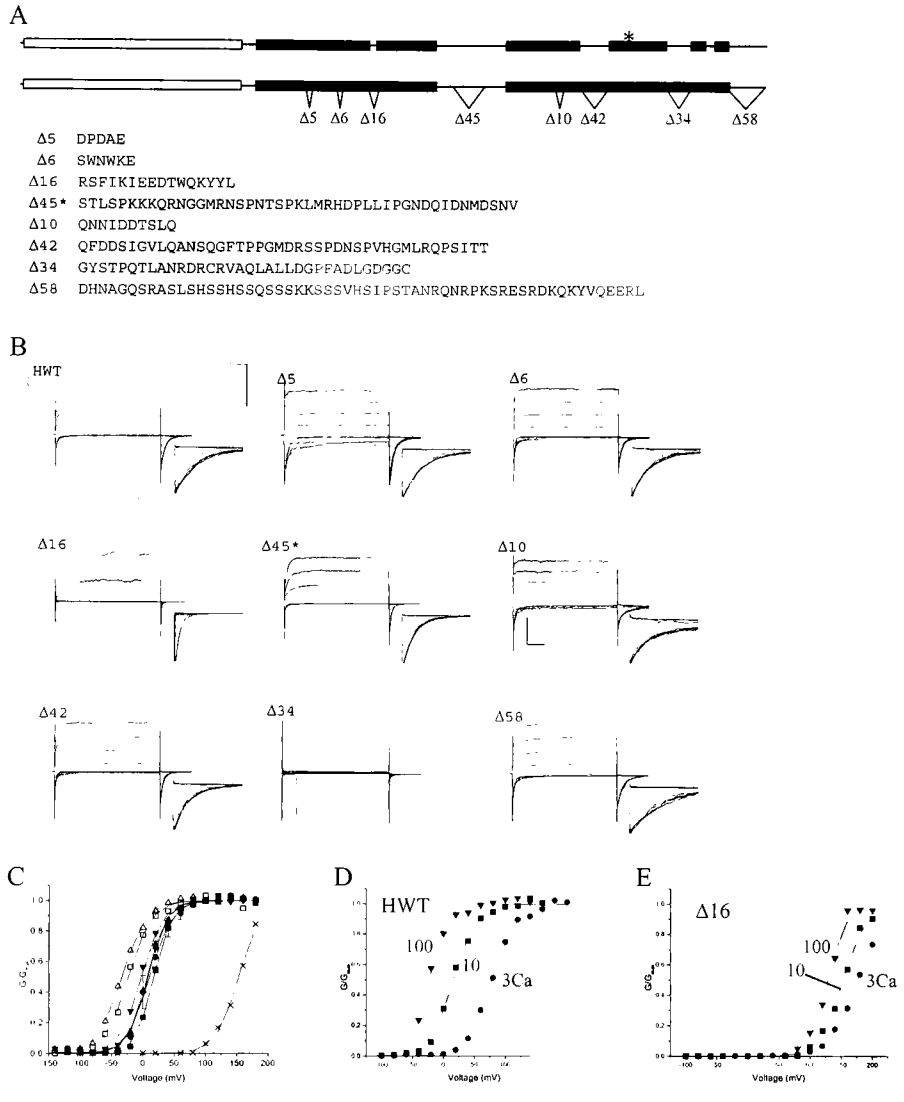

Figure 12 Loop deletions in HBK. (A) Position of loops tested for deletion along schematic of RCK domain model aligned with primary domain model of HBK. Loops are labeled according to number of amino acids, e.g., Δ5 is a five amino acid loop. Below the schematic the sequence of each of the loops is given. (B) Macrocurrents elicited by a series of 20mV voltage steps on inside-out patches exposed to 10μM Ca^{2+} from wild type (HWT) and deletion mutant channels. The displayed activation traces result from voltages ranging -140mV to +80mV; except Δ16, -100mV to +140mV. Tail currents (insets) result from voltages ranging -140mV to +160mV; expect Δ5, -160mV to +80mV, and Δ16, -100mV +200mV Scale bars indicate 2nA vertical, 5msec horizontal, and 1msec horizontal for insets. (C) Normalized G-V curves (see Methods: Electrophysiology) for wild type and deletion mutants at 10μM Ca^{2+}: HWT (solid circle), Δ5 (open up triangle), Δ6 (closed down triangle), Δ16 (cross), Δ45 (solid square), Δ10 (open square), Δ42 (solid up triangle), Δ58 (solid diamond). (D) G-V curves for HWT at a range of $[Ca^{2+}]$: 3μM (cirlce), 10μM (square), and 100μM (down triangle). (E) G-V curves for Δ16 over the same range of $[Ca^{2+}]$. *Note, Δ45 was tested by co-injection (see Fig. 13 and text) not by deletion from a single construct.

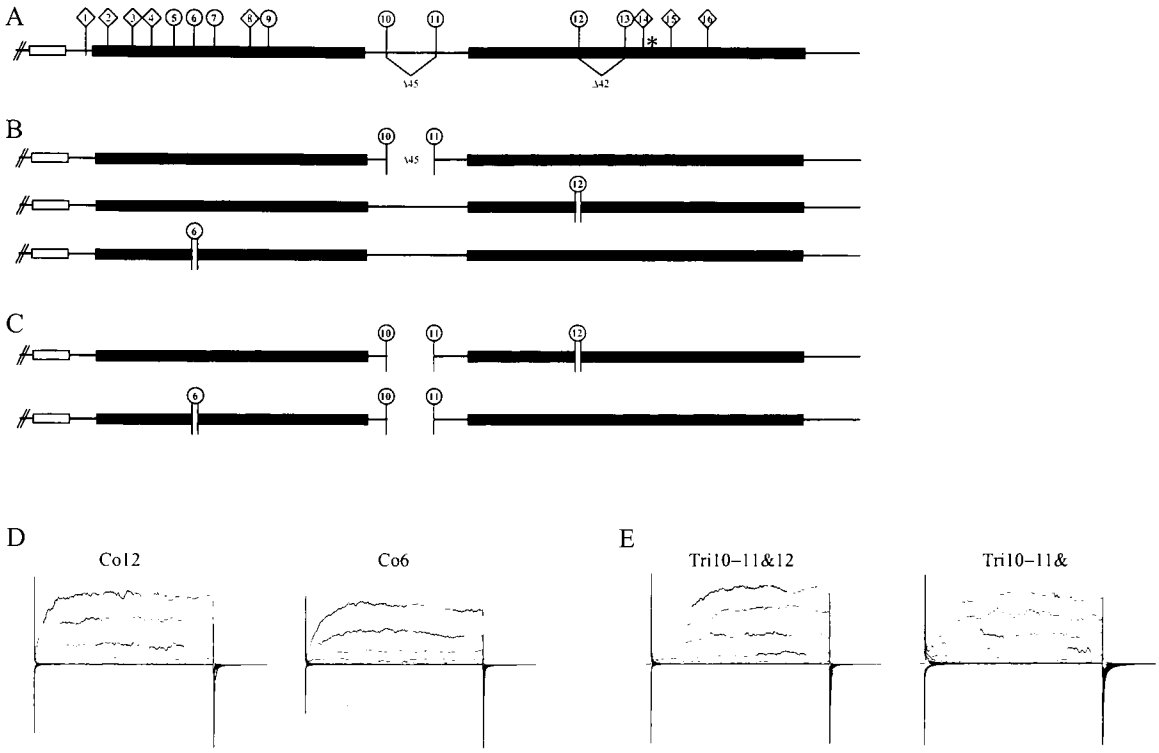

Figure 13 Co-injection of HBK constructs. (A) Dissection points are indicated by numbered posts along the schematic of the RCK domain model of HBK: circles are dissection points that successfully produced channel currents upon co-injection, diamonds are points that failed to produce currents. Asterisk denotes position of Ca^{2+} bowl. (B) Schematics of example co-injection constructs around positions 10-11, 12 and 6. (C) Tri-injection constructs using positions 10-11&12, and 10-11&6. (D) Macrocurrents from co-injections around positions 12 and 6. Currents displayed for Co12 were elicited by -100mV to +140mV voltage steps on cell-attached patches 2 days after co-injection of RNA. Co6 currents are from -100mV to +200mV, cell-attached, day 6. (E) Macrocurrents from tri-injections using positions 10-11&12 and 10-11&6. Tri10-11&12 currents are from -100mV to +200mV, cell-attached, day 4. Tri10-11&6 currents are from -100mV to +200mV, cell-attached, day 5. Scale: 0.5nA, 5msec.

A

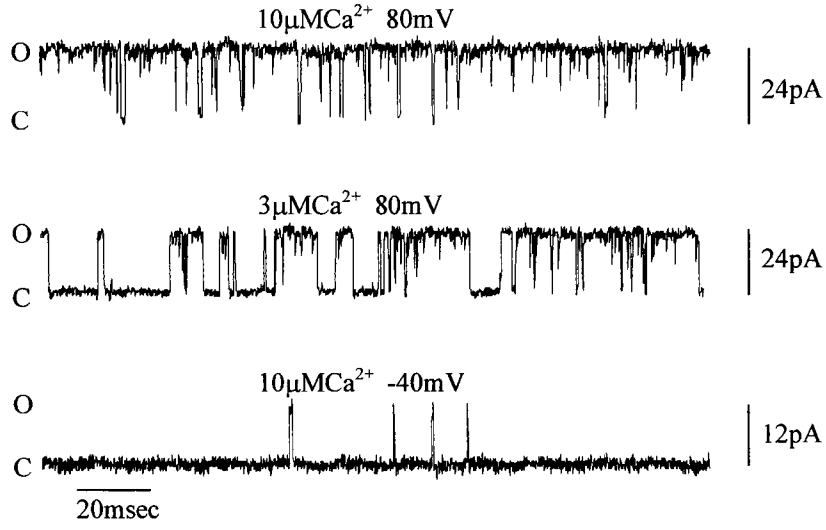

B

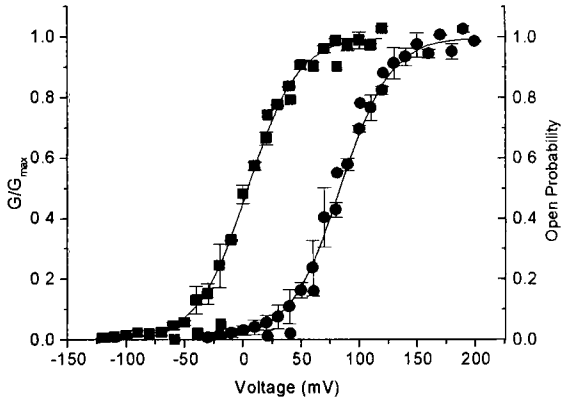

Figure 14. Single channel analysis of mutant K448D. (A) Representative samples of single channel currents from a single patch at different [Ca^{2+}] and voltage indicated above each trace. Upward deflections are openings (the trace at -40mV was vertically flipped to maintain the orientation). Open probabilities were calculated from 8-10 seconds of data over a range of [Ca^{2+}] and voltage. The top trace represents a Po of 0.90, middle trace 0.55 and bottom trace 0.02. (B) Single channel analysis (red) plotted with macrocurrent analysis (black) for the mutant K448D at two different [Ca^{2+}]: 3μM (circles) and 10μM (squares). The macrocurrent analysis involves a normalization and fit (black lines) by a simple Boltzmann equation (see Methods: Electrophysiology).

A

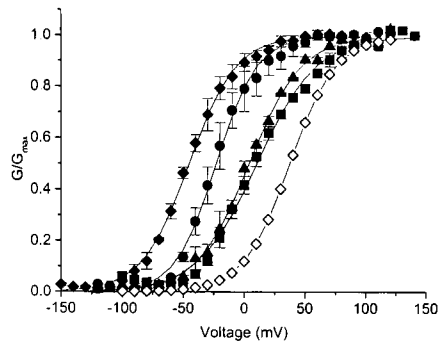

B

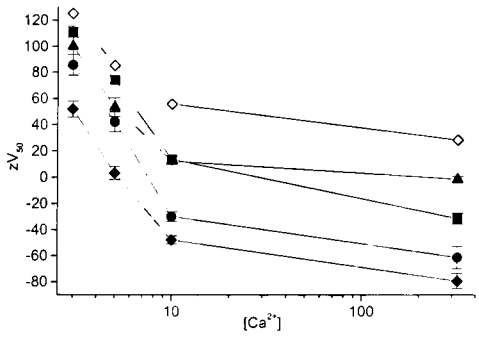

Figure 15 Double mutant cycle on predicted salt-bridging residues in HBK. (A) Normalized G-V curves for wild type and mutants at 10μM Ca^{2+}: HWT (circle), K448D (triangle), D481K (square), double mutant K448D/D481K (solid diamond), additive single mutants (open diamond). (B) Plot of zV_{50} over a range of $[Ca^{2+}]$ (3μM, 5μM, 10μM, 300μM) for wild type and mutants (same symbols). Error bars indicate s.e.m. calculated from n=3, except for K448D (n=2).

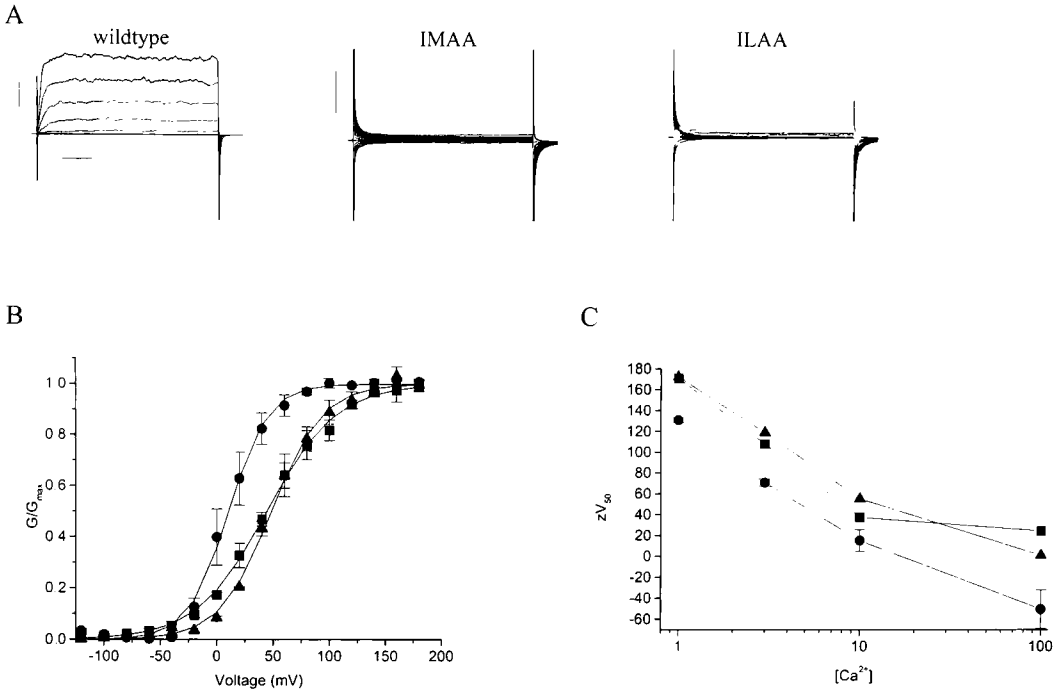

Figure 16 Point mutations at the αD interface of HBK. (A) Current expression from wild type and interface mutants, IMAA (I441A/M442A) and ILAA (I821A/L822A), of RCK1 and RCK2 of HBK. Macrocurrents of wild type 2 days following RNA injection (scale: 5nA, 5msec). Currents of IMAA at day 4 and ILAA at day 2 (scale: 0.5nA vertical). (B) Normalized G-V curves for wildtype and mutants at 10μM Ca^{2+}: HWT (circle), I445A (square), L825A (triangle). (C) Plot of zV_{50} over range of [Ca^{2+}] (1μM, 3μM, 10μM, 100μM) for wild type and mutants (same symbols). Error bars indicate s.e.m. calculated from n=2.

A

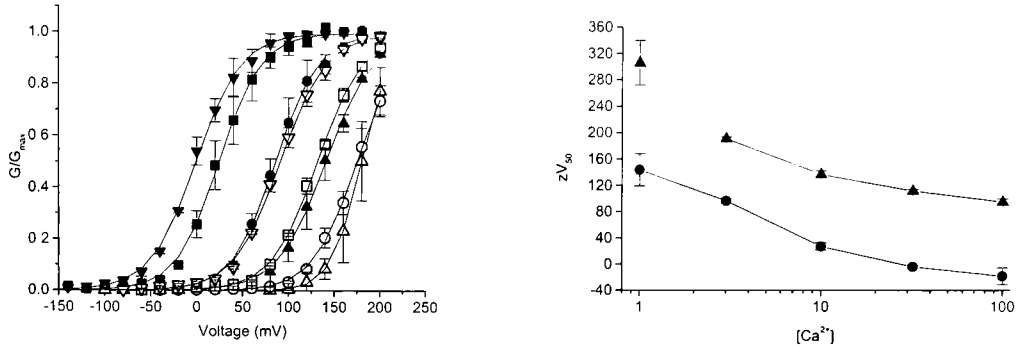

B

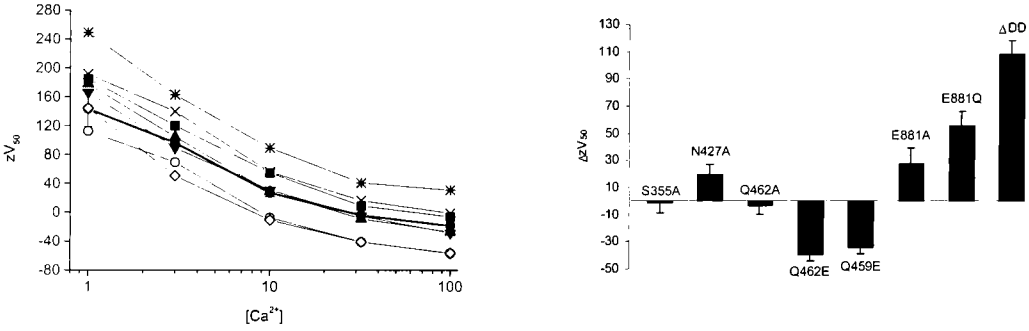

Figure 17 Ca^{2+}-binding residues in HBK. (A) Effect of deletion within Ca^{2+} bowl on sensitivity and activation. (Left) Overlapping sets of G-V curves for wild type (solid symbols) and deletion mutant ΔDD (D894, D895; open symbols) over a range of $[Ca^{2+}]$: 1μM (up triangles), 3μM (circles), 10μM (squares), 100μM (down triangles). (Right) Plot of zV_{50} over same range of $[Ca^{2+}]$: HWT (circle), ΔDD (triangle). Error bars indicate s.e.m. calculated from n=2. (B) Effects of mutations to potential Ca^{2+}-binding residues. (Left) Plot of zV_{50} over same range of $[Ca^{2+}]$: HWT (solid circle), N427A (solid square), S335A (solid up triangle), Q459E (open circle), Q462E (open diamond), Q462A (solid down triangle), E881A (cross), E881Q (asterisk). (Right) Histogram of the effect of mutation relative to wild type (ΔzV_{50}) averaged over a range of $[Ca^{2+}]$: 3-100μM.

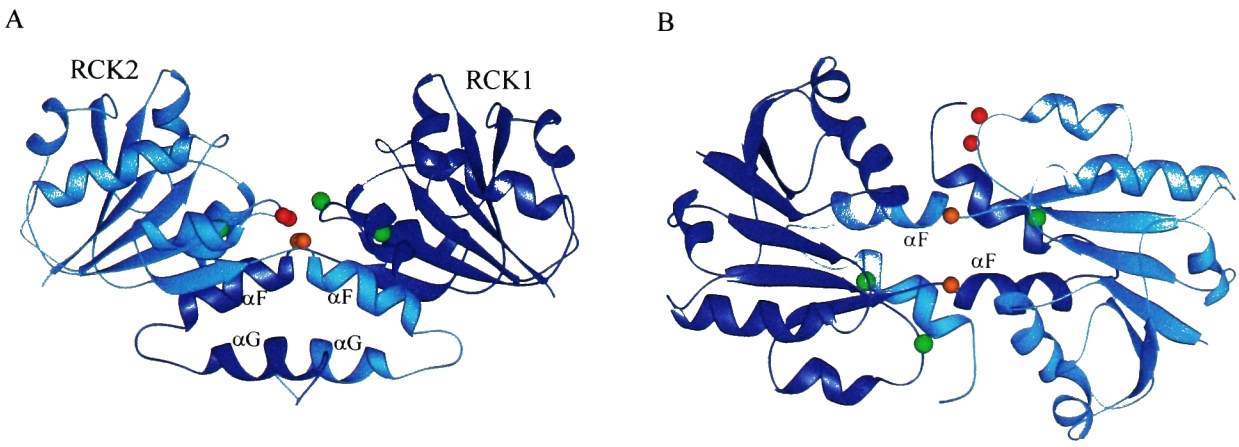

Figure 18 Ca^{2+} binding model for HBK. (A) A pair of RCK domains from the octameric ring of MthK as a model for a given pair of RCK domains in HBK: RCK1 (dark blue) and RCK2 (light blue). Orange spheres represent the hinge positions of the flexible interface between the initial α-β-α layered domain and the αF-αG element (the subdomain, post αG, has been removed for visual clarity). Red spheres represent the position of the Ca^{2+} bowl in the loop between βE and αE. Green spheres represent the other contributors to Ca^{2+} sensitivity within the binding cleft: Q459 and Q462 of RCK1 and E881 of RCK2. (B) Same structure and color-coded positions from a different perspective, looking down the binding clefts to the flexible interface.

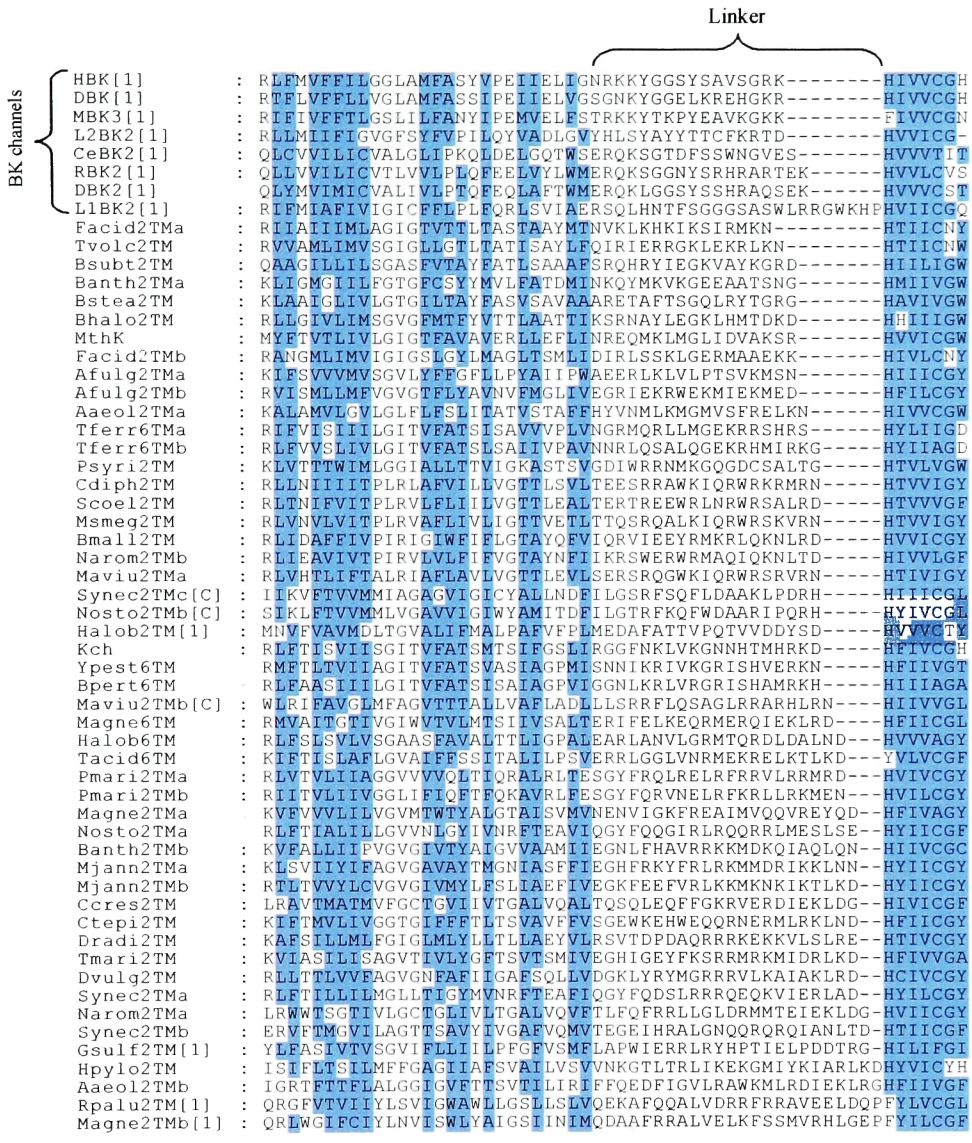

Figure 19 Multiple sequence alignment of linker region connecting K^+ channel domains to RCK domains. The alignment begins at the last TM helix, covers the linker region and ends at the first beta strand of the RCK domain (βA). Sequences are ordered by length of linker (labeled bracket top) within two groups: BK channels (labeled bracket left) and prokaryotic K^+ channels. Conservation at 80% similarity is shown in blue. Appendix B contains the complete alignment and sequence identities.

A

WT: NRKKYGGSYSAVSGRK

-1. NRKKYG-SYSAVSGRK
-2: NRKKYG--YSAVSGRK
+1. NRKKY**S**GGSYSAVSGRK
+2: NRKKY**GS**GGSYSAVSGRK
+3: NRKKY**GGS**GGSYSAVSGRK
+6: NRKKY**GGSGGS**GGSYSAVSGRK

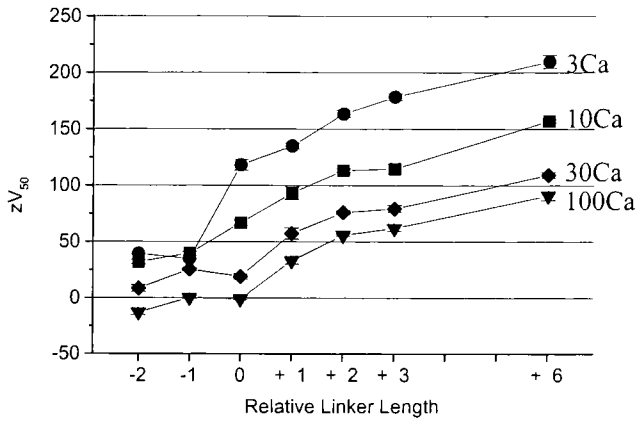

B

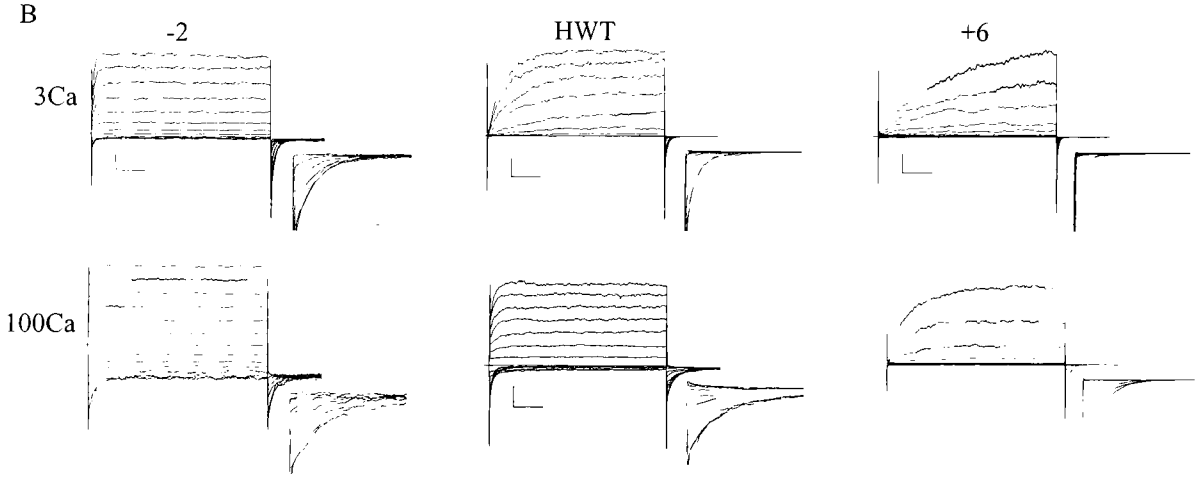

C

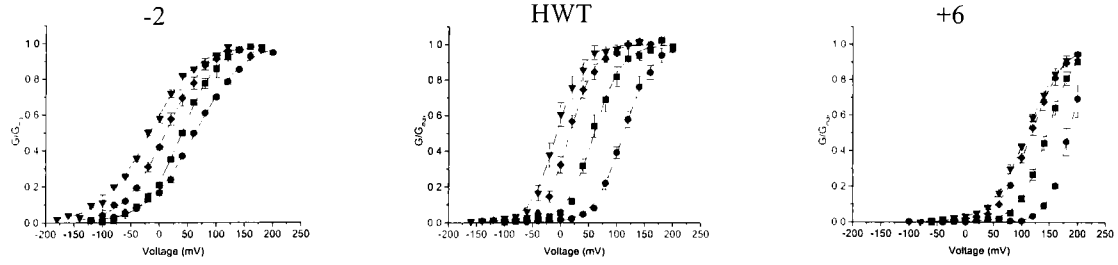

Figure 20 Linker analysis in HBK. (A) List of deletions (dash) and insertions (bold) made to linker region: wild type is underlined; deletion of 1 through insertion of 6 are labeled -1 through +6. Plot of zV_{50} for wild type (0), deletions (-1, -2) and insertions (+1, +2, +3, +6) at four $[Ca^{2+}]$: 3μM (circle) 10μM (square), 30μM (diamond), 100μM (down triangle). (B) Macrocurrent traces showing activation and deactivation (insets) in response to a series of voltage steps. Arranged in columns and rows: first column is data for -2, second column for wild type, third column for +6; first row is data collected in 3μM Ca^{2+}, second row is 100μM Ca^{2+} Scale: 2nA, 5msec, and 1msec for insets. (C) G-V curves for -2, wild type, and +6 for a range of $[Ca^{2+}]$: same symbols at in (A). Error bars indicate s.e.m. calculated from n=2-5.

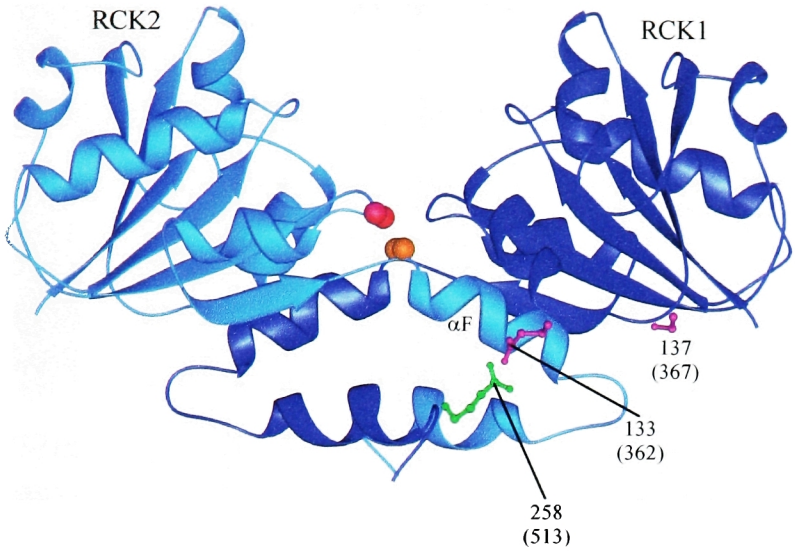

Figure 21 Structural interpretation of Ca^{2+} activation data. Residues having a significant effect on the Ca2+ activation mechanism in BK are mapped onto the RCK domain model. M513 is represented by the corresponding residue in the MthK sequence, E258 (green). D362 and D367 are represented by MthK E133 and S137 (magenta). The interfacial element, αF, of the second RCK domain (light blue) is included in Region C used in tail chimeras. The loop corresponding to the Ca2+ bowl is indicated by a pair of red spheres. Hinge positions about which relative conformational changes have been observed are indicated by orange spheres.

APPENDIX A

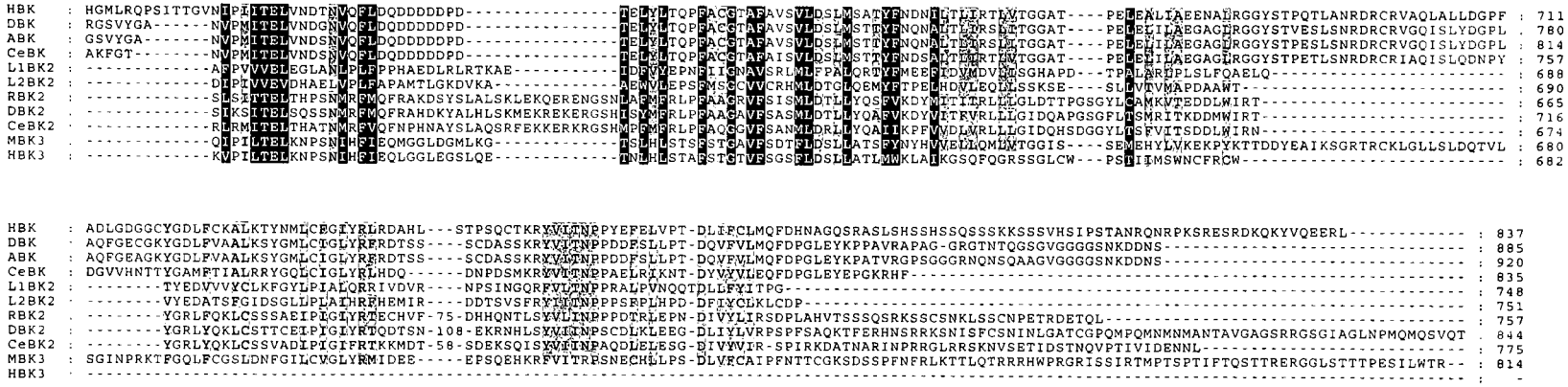

Appendix A Multiple sequence alignment of diverse BK channel family members: HBK (*Homo sapiens* Slo1, GI:26638650), DBK (*Drosophila melanogaster* Slo1, GI:321029), ABK (*Anopheles gambiae* Slo1, GI:21296709), CeBK (*Caenorhabditis elegans* Slo1, GI:25154297), L1BK2 (*Leishmania major* Slo2, GI:11466170), L2BK2 (*Leishmania major* Slo2, GI:11466171), RBK2 (*Rattus norvegicus* Slo2, GI:1117789), DBK2 (*Drosophila melanogaster* Slo2, GI:24652410), CeBK2 (*Caenorhabditis elegans* Slo2, GI:25147254), MBK3 (*Mus musculus* Slo3, GI:6680542), HBK3 (*Homo sapiens* Slo3, GI:20381097). Alignment begins at K^+ channel signature sequence and ends at protein C-terminus. Sequence similarity is indicated at 100% (dark shade) and 80% (light shade). Note that the HBK3 sequence is truncated, either naturally or by sequencing error, and was thus excluded from the calculation of similarity in this region for the purposes of determining primary domain model from conservation pattern (see Fig. 3). Numbers within the alignment indicate large, insertions of random sequence. These insertions were also taken into consideration in primary domain determination. Line numbers are relative to the alignment as presented.

APPENDIX B

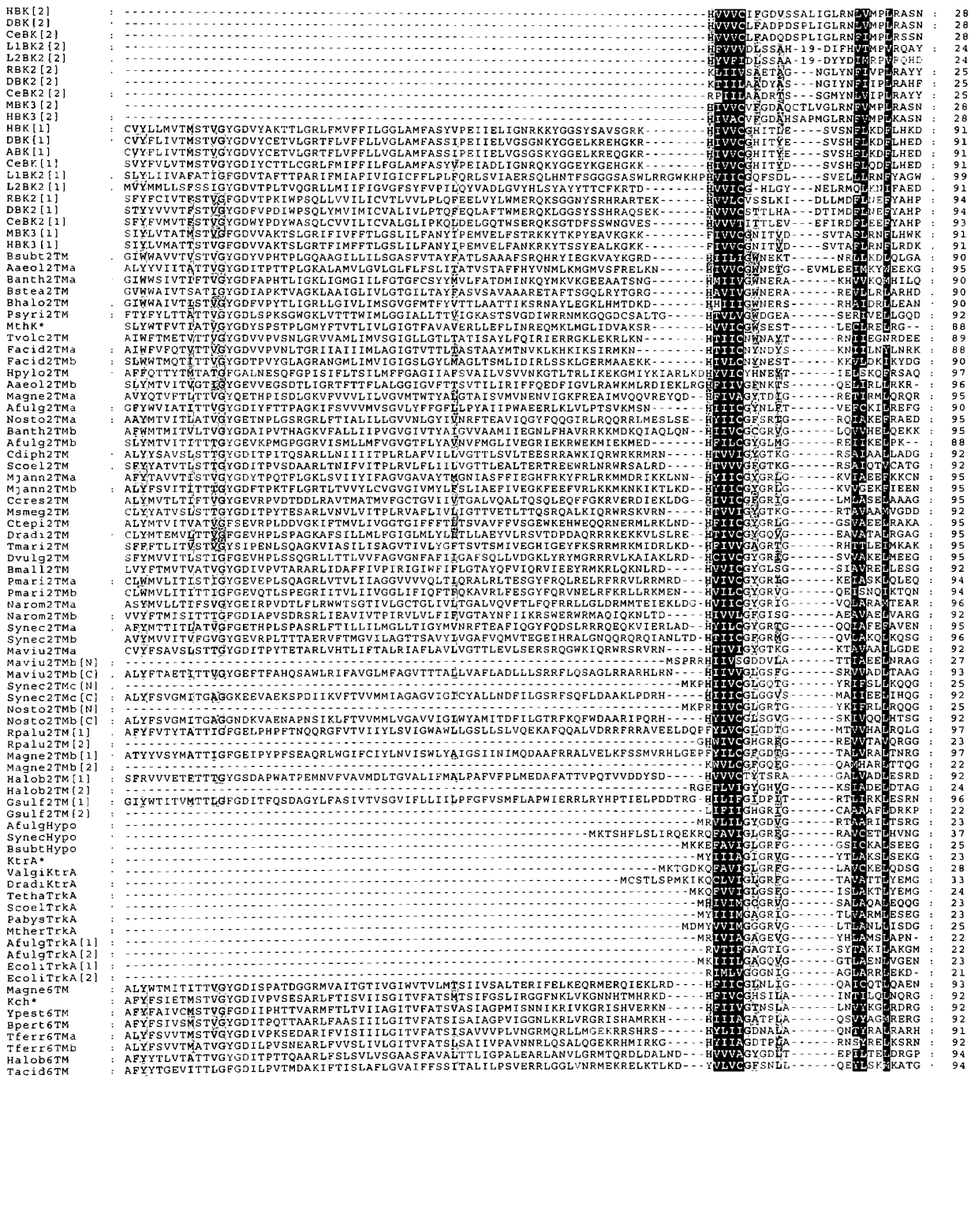

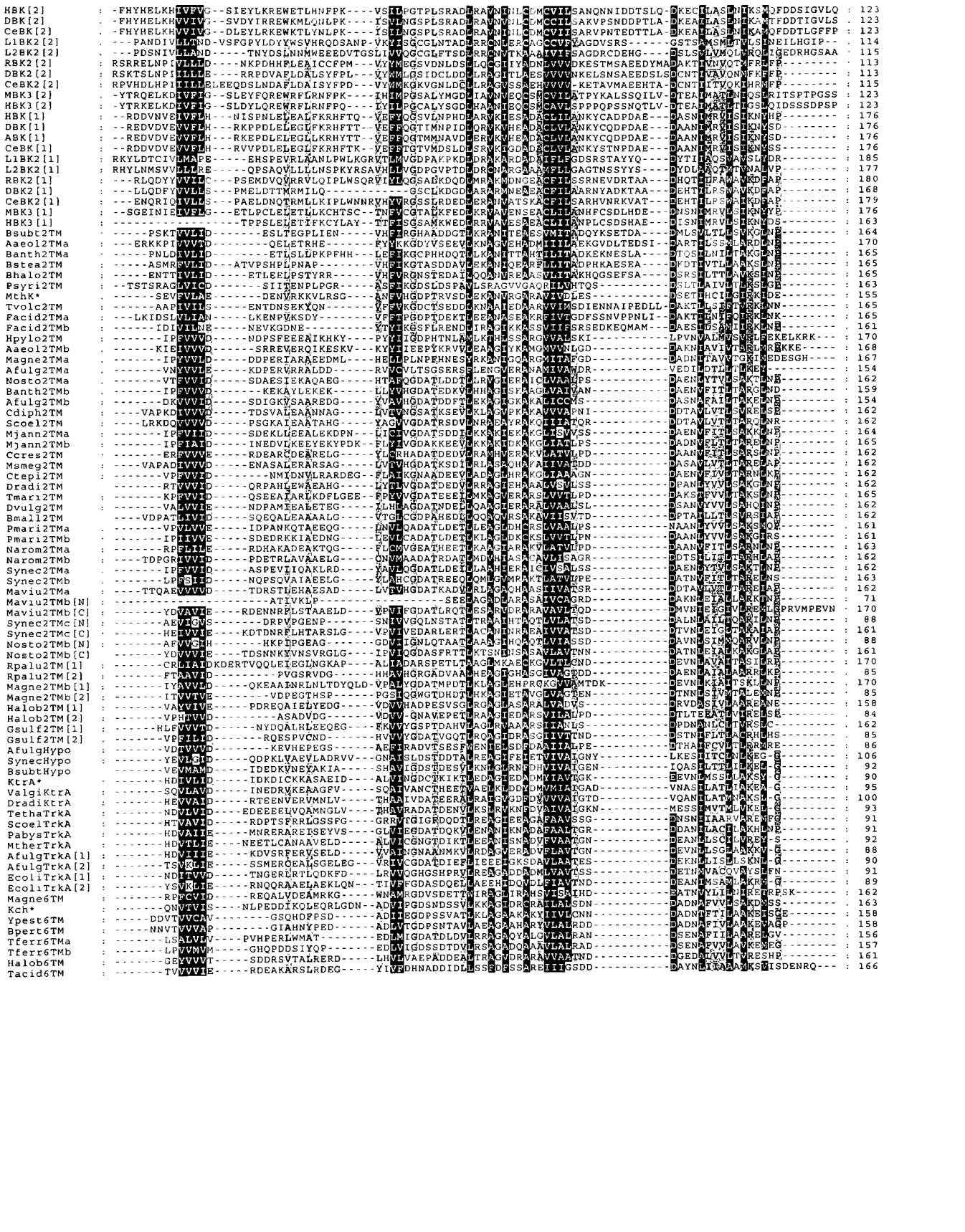

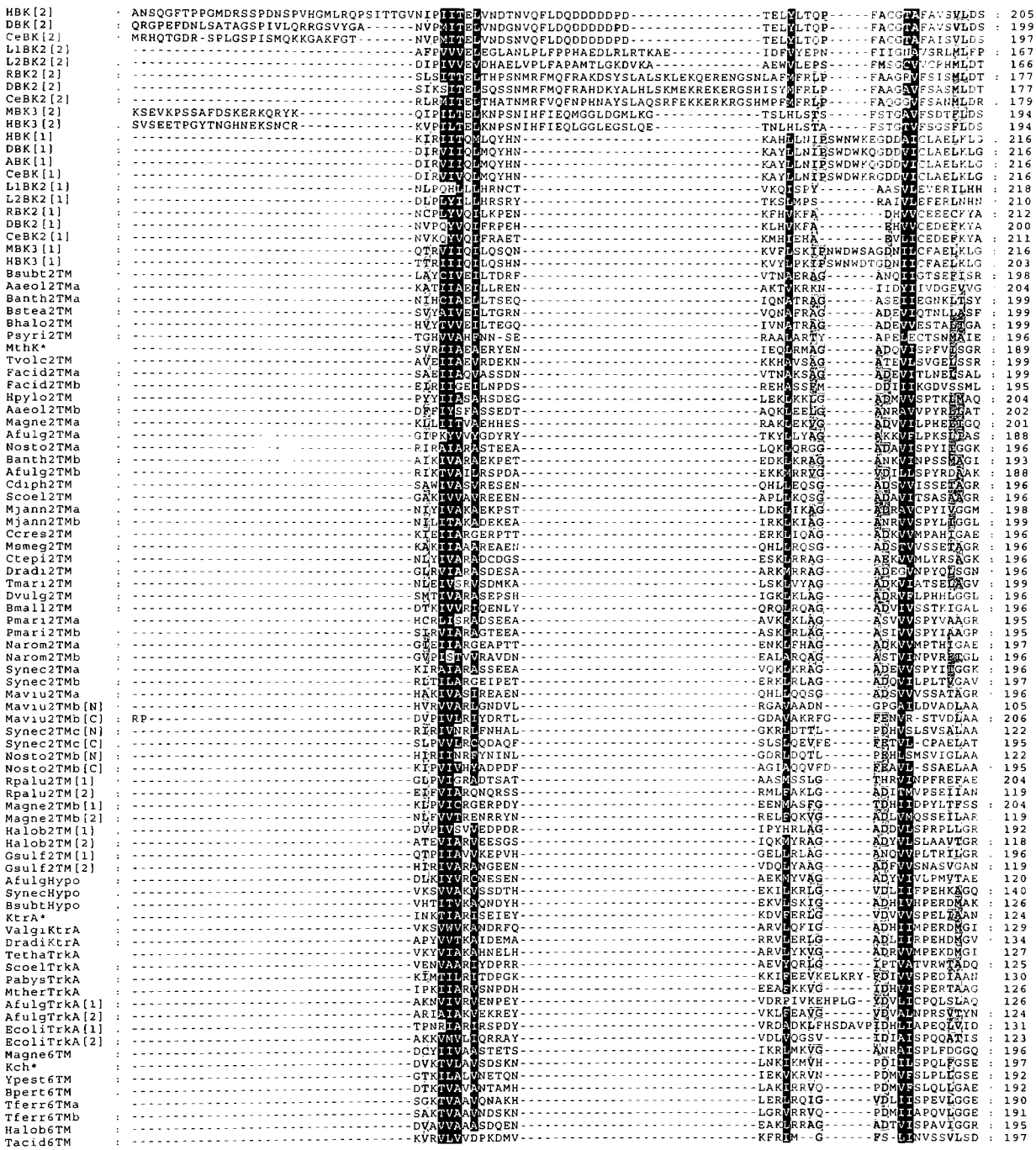

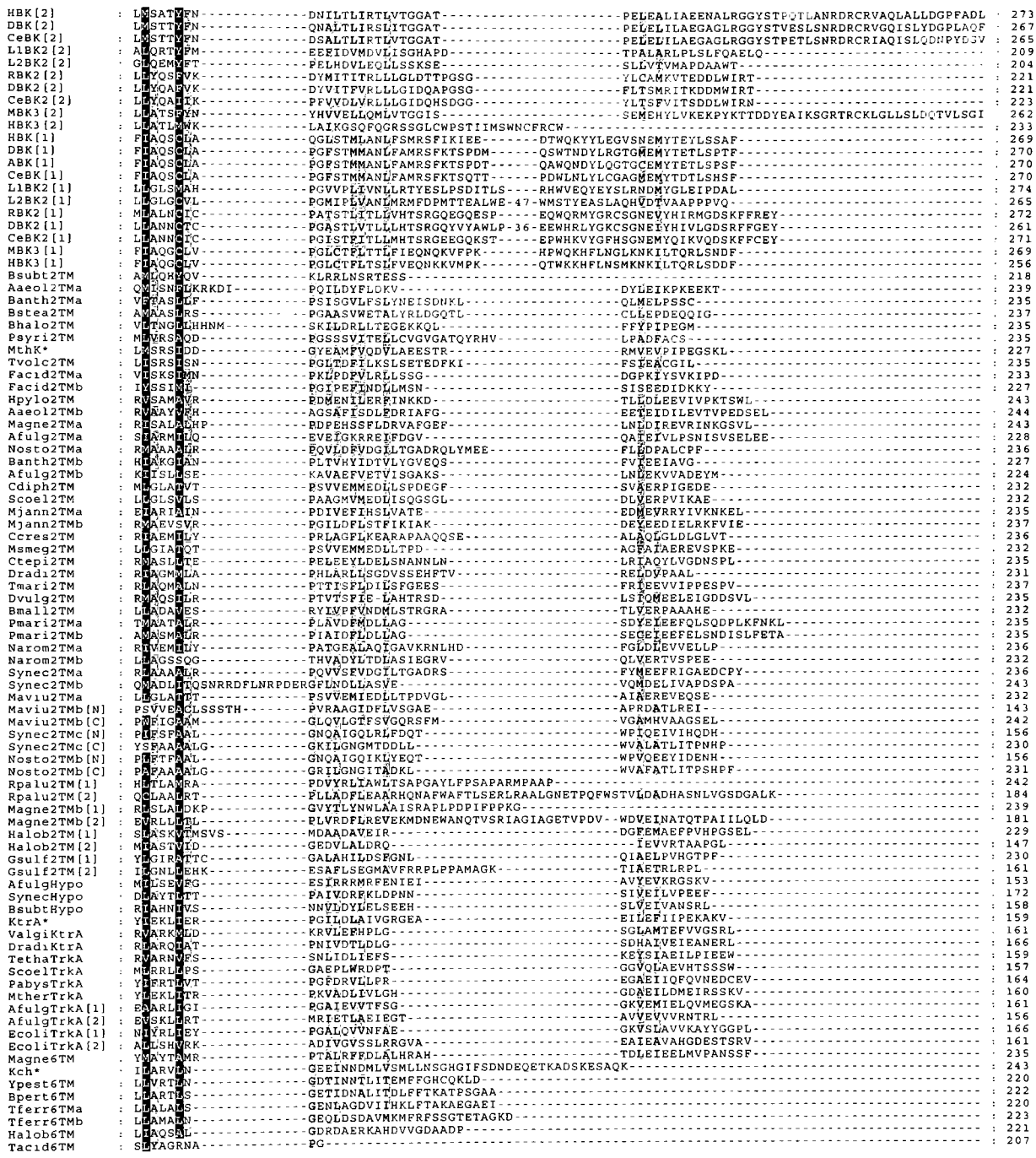

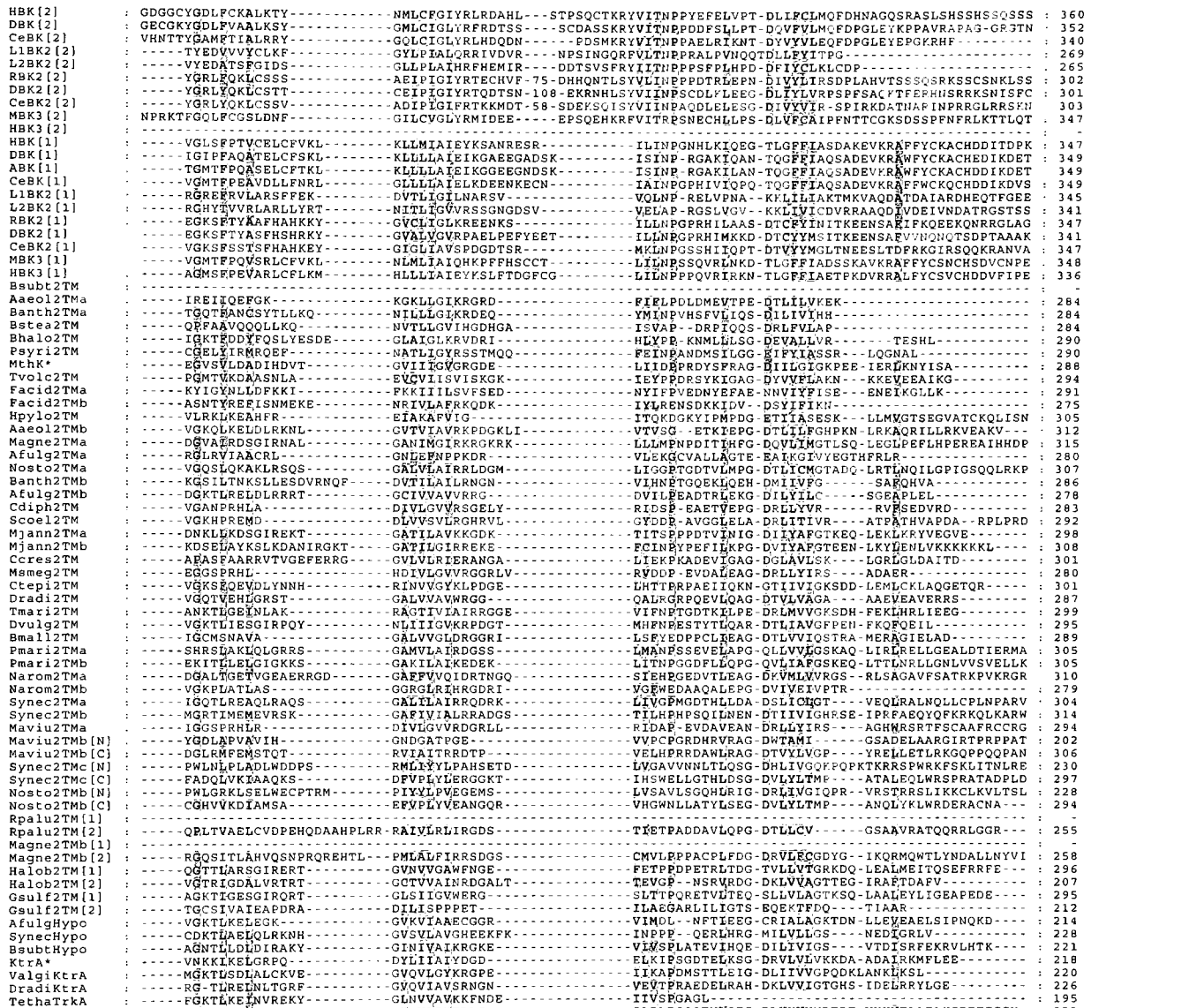

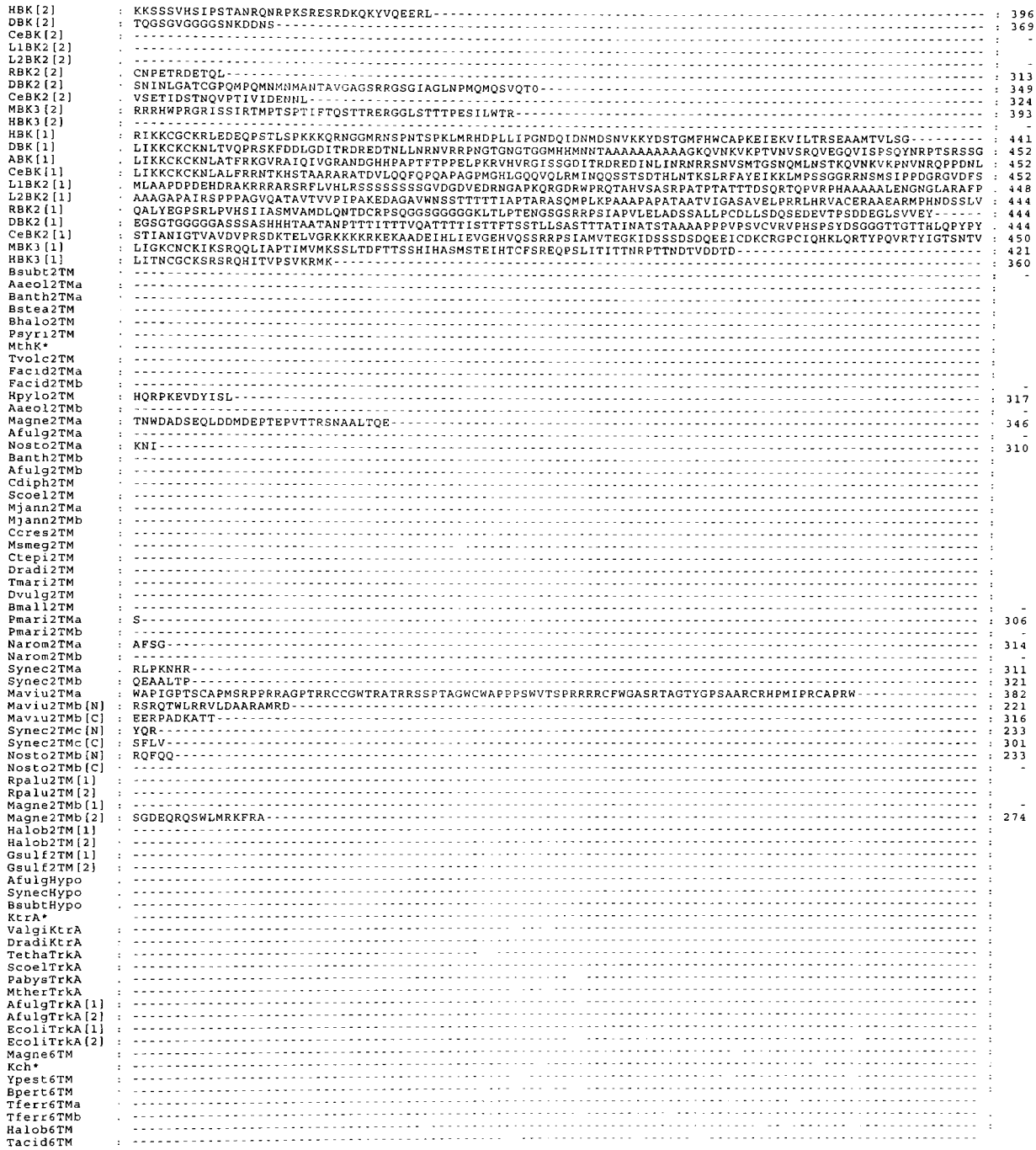

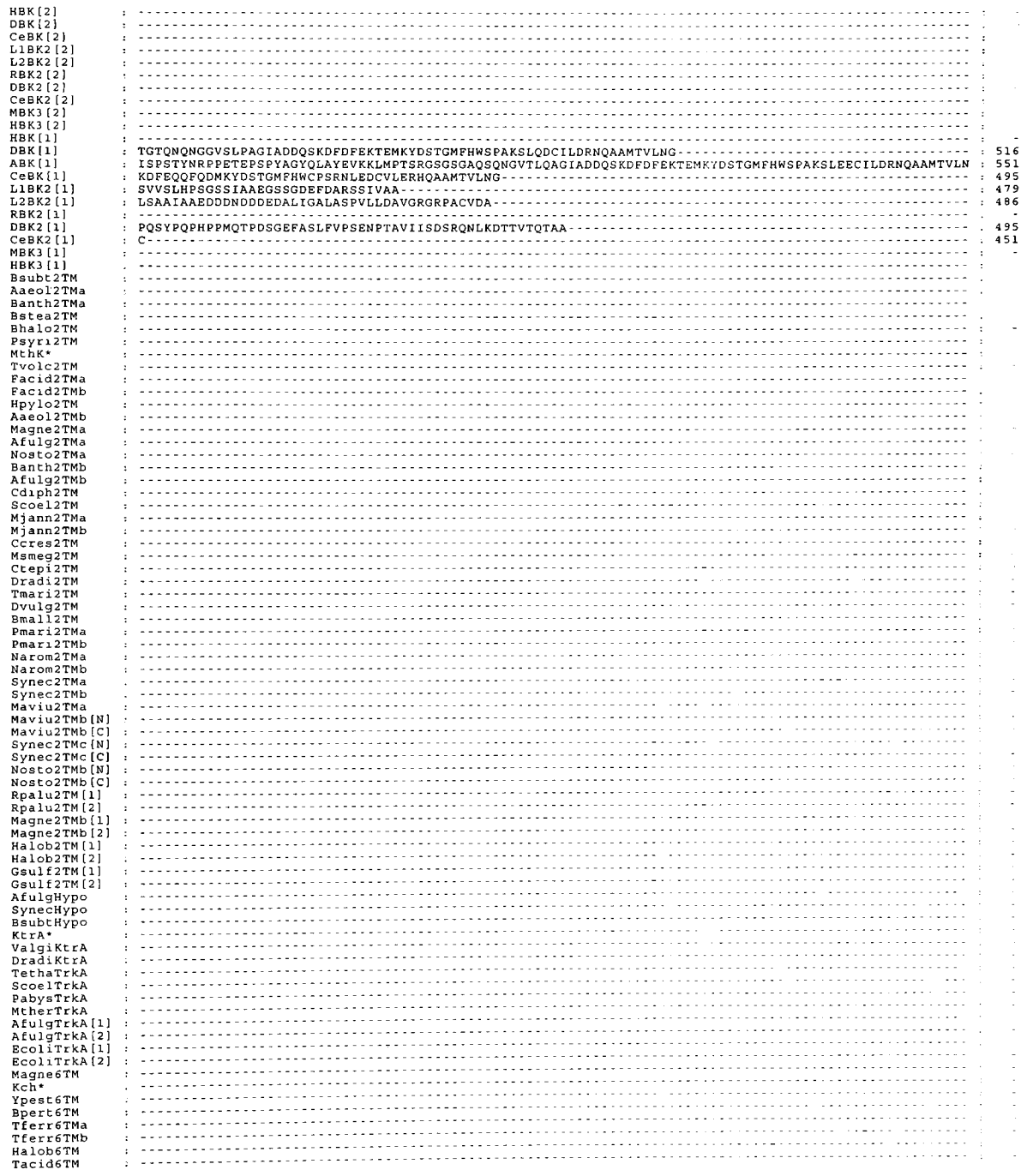

Appendix B Multiple sequence alignment of available RCK domains of low redundancy (<65% seqID), including those from eukaryotic BK channels, 2TM and 6TM prokaryotic K^+ channels, K^+ transport system domains, and proteins annotated as hypothetical: **BK channels**: sequences are identified in Appendix A, **2TM prokaryotic channels**: Bsubt2TM (GI:7475768), Aaeol2TMa (GI:15606902), Banth2TMa (GI:21397377), Bstea2TM (gnl|UOKNOR_1422|bstear_Contig1568), Bhalo2TM (GI:10175963), Psyri2TM (gnl|TIGR_323| psyring_5332), MthK (GI:7482789, *PDB:1LNQ), Tvolc2TM (GI:14325256), Facid2TMa (gnl|DOE_97393| Contig155.revised.gene126.protein), Facid2TMb (gnl|DOE_97393|Contig155.revised.gene29.protein), Hpylo2TM (GI:15645117), Aaeol2TMb (GI:15605833), Magne2TMa (gnl|DOE_156889|Contig232.revised. gene4.protein), Afulg2TMa (GI:11498322 + GI:11498323), Nosto2TMa (GI:17130425), Banth2TMb (gnl |TIGR_1392|banth_1526), Afulg2TMb (GI:11499263), Cdiph2TM (gnl|Sanger_1717|cdiph_Contig38), Scoel2TM (GI:7481024), Mjann2TMa (GI:1498918), Mjann2TMb (GI:1592000), Ccres2TM (gnl|TIGR| C.crescentus_4943), Msmeg2TM (gnl|TIGR_1772|msmeg_3275), Ctepi2TM (gnl|TIGR|C.tepidum_3495), Dradi2TM (GI:15807327), Tmari2TM (GI:15643815), Dvulg2TM (gnl|TIGR_881| dvulg_1531), Bmall2TM (gnl|TIGR_13373|bmallei_102), Pmari2TMa (gnl|DOE_74547|Contig476.revised.gene343.protein), Pmari2TMb (gnl|DOE_59919|Contig26.revised.gene1290.protein), Narom2TMa (gnl|DOE_48935|Contig207. revised.gene40.protein), Narom2TMb (gnl|DOE_48935|Contig211.revised.gene36.protein), Synec2TMa (GI: 16329750), Synec2TMb (GI:16332066), Maviu2TMa (gnl|TIGR|M.avium_34), Maviu2TMb[N]&[C] (gnl |TIGR|M.avium_303), Synec2TMc[N]&[C] (GI:16331097), Nosto2TMb[N]&[C] (GI:17129785), Rpalu2TM[1]&[2] (gnl|DOE_1076|Contig59.revised.gene1883.protein), Magne2TMb[1]&[2] (gnl |DOE_156889|Contig314.revised.gene5.protein), Halob2TM[1]&[2] (GI:10580209), Gsulf2TM[1]&[2] (gnl |TIGR_35554|gsulf_2947), **Isolated RCK domains**: AfulgHypo (GI:2649897), SynecHypo (GI:1001359), BsubtHypo (GI:732401), KtrA (GI:15669293, *PDB:1LSS), ValgiKtrA (GI:3288678), DradiKtrA (GI: 15806669), TethaTrkA (GI:2581796), ScoelTrkA (GI:2815362), PabysTrkA (GI:5459187), MtherTrkA (GI: 15679276), AfulgTrkA[1]&[2] (GI:11498444), EcoliTrkA[1]&[2] (GI:15803817), **6TM prokaryotic channels**: Magne6TM (gnl|DOE_156889|Contig441.revised.gene50.protein), Kch (GI:16129211, *PDB:1ID1), Ypest6TM (GI:15980654), Bpert6TM (gnl|Sanger_520|B.pertussis_Contig305), Tferr6TMa (gnl|TIGR| t_ferrooxidans_2924), Tferr6TMb (gnl|TIGR|t_ferrooxidans_2975), Halob6TM (GI:10581294), Tacid6TM (GI: 10640775). **Note**: [1] & [2] denote first and second RCK domains following a channel domain in tandem; [N] & [C] denote N-terminal and C-terminal RCK domain relative to a channel domain. Alignment begins at the K^+ channel signature sequence and ends at the completion of the RCK domain. Secondary RCK domains ([2]), N-terminal RCK domains [N], and isolated RCK domains (Hypo, KtrA, TrkA) begin at the initiation of the RCK domain in the sequence alignment. Singular RCK domains (channel associated or isolated), secondary RCK domains ([2]), and C-terminal RCK domains ([C]) end at the protein C-terminus. N-terminal RCK domain sequences ([N]) end just prior to the first TM helix of the channel domain and primary RCK domain sequences ([1]) end just prior to the beginning of the second RCK domain. Notice the segregation (from top to bottom) of BK channels ([2] & [1] domains), 2TM prokaryotic K^+ channels, isolated domains, and 6TM prokaryotic K^+ channels. Within the 2TM prokaryotic K^+ channels, sequences are further subdivided: those without the

canonical NAD(+)-binding motif in the RCK domain (Bsubt2TM Nosto2TMa), those with the motif (Banth2TMb - Maviu2TMa), sequences with N- and C-terminal RCK domains ([N]&[C]), and sequences with tandem C-terminal RCK domains ([1]&[2]). Also note that the NAD(+)-binding motif is found in all of the isolated RCK domains (Hypo, KtrA, TrkA), but is not found in any of the 6TM or BK channel sequences. Sequence similarity is indicated at 90% (dark shade) and 65% (light shade). A number of sequences were found to be truncated post αG: 6TM prokaryotic K^+ channels (exception: Magne6TM), Bsubt2TM, Rpalu2TM[1], Magne2TMb[1] and HBK3[2]. Truncated sequences were excluded from the calculation of similarity in this region for the purposes of determining the pattern of conservation for RCK domains. Line numbers are relative to the alignment as presented.

APPENDIX C

A recent report states that the removal of the entire C-terminus, from the end of S6 onwards, results in wild type-like BK currents with normal voltage and Ca^{2+} dependence (Piskorowski and Aldrich, 2002). This claim is clearly at odds with the body of literature that has demonstrated the relevance of the C-terminal domains to Ca^{2+} activation (see References for a short list) and it specifically conflicts with the model presented here for the C-terminus as the structural and functional unit of the Ca^{2+} activation mechanism in BK. The evidence supporting the claim that the C-terminus is not necessary for Ca^{2+} activation, however, is obscured by a number of issues.

The main issue that makes the results difficult to assess is the extremely low expression of observed BK currents in their experiments. This is an important issue because of a low level of endogenous BK channels in cell types used for the assay of exogenous BK current, e.g., *Xenopus* oocytes. Endogenous expression of BK currents is commonly seen in *Xenopus* oocytes (Krause, Foster & Reinhart, Neuropharmacology (1996) 35(7): 1017-1022); BK channel mRNA are found in HEK cells (Larry Salkoff, personal communication); and BK channels are prominently expressed in the follicle cells of *Xenopus* oocytes (see observations below). The number of observations as reported (typically 2-5 channels per patch) and the high variability in the observations (later communicated to be dependent on frog batch) are not, by themselves, convincing evidence of exogenous channel current expression from an injected construct.

In an attempt to reproduce the finding, I assessed the expression of the truncated construct (*truncated Mslo*, provided by the Aldrich lab) and a similarly truncated human BK construct (*truncated HBK*) in parallel with the expression of endogenous BK from

uninjected control oocytes. I controlled for batch-dependence and any potential temporal variables by following a strict protocol of parallel surveys of injected and uninjected oocytes. In other words, I searched for BK channel currents in the uninjected oocytes *as hard* as I did in the injected oocytes. Equal sampling is, of course, crucial to any survey making claims about the significance of a signal relative to the noise. The results of this survey and the observation of 2-9 BK channels per patch from an endogenous *Xenopus* source are described in detail in the next two sections:

BK current expression from uninjected and truncation-injected oocytes

Three batches of oocytes from independent dissections were injected with truncated constructs. Within each batch I pulled numerous patches from uninjected and truncation-injected oocytes over a period of 1 to 4 days following injection (2-5 days following dissection). Out of a total of 370 patches I observed single channel BK currents in 12 patches:

Batch 1: *truncated HBK* constructed by removing sequence following VAL339

	oocytes	patches	BK singles
Uninjected	7	49	0
Truncation	5	50	0

(0 of 99 patches)

Batch 2: *truncated Mslo* provided by Aldrich

	oocytes	patches	BK singles
Uninjected	3	12	1
Truncation	7	70	0

(1 of 82: ~1%)

Batch 3: *truncated Mslo* provided by Aldrich (same as in Batch2)

	oocytes	patches	BK singles
Uninjected	7	70	4
Truncation	9	119	7

(4 of 70: ~6%; and 7 of 119: ~6%)

The level of endogenous BK channel expression varied across the three batches of oocytes (0-6%). I did not, however, find a significant increase in the expression of BK currents due to the injection of truncated constructs. The preparation and injection of wildtype constructs served as positive controls for each RNA preparation and for the viability of each batch of oocytes. In each batch full-length, wildtype constructs gave significant currents (day1: 0.4 1.0nA of maximum current, day2: 2 14nA, day3: too much current to measure).

Significant densities of BK channels found on partially digested oocytes

I was able to obtain patches on uninjected oocytes containing 2-9 BK channels. Incomplete digestion of the follicle layer by collagenase treatment and the subsequent incubation of oocytes with an intact or partial follicle layer provide the conditions for finding significant densities of BK channels. Removing the follicle cells just prior to patching reveals regions of local adhesion between the vitelline matrix and the plasma membrane of the oocyte where the vitelline does not separate and "fall away" easily. These regions can in fact appear to be devitellinized, and, unlike vitelline under normal conditions, patches can readily be formed on these regions. Patches obtained in this manor consistently contained 2-9 BK channels. This was observed in three separate batches of oocytes in a total of 13 patches.

Interestingly, the vitelline layer could be removed from such regions and patches taken from the newly devitellinized regions contained either no BK channels (for uninjected oocytes) or large macrocurrents (for wildtype-injected oocytes). It is therefore likely that what was actually being patched were residual follicle cells. Follicle cells form gap junctions with the plasma membrane of the oocyte through the vitelline matrix and the adhesion between vitelline and plasma membrane has previously been related to insufficient digestion of the follicle (Choe & Sackin, Pflugers Arch (1997) 433(5): 648-52). Furthermore, follicle cells are known to express BK channels (Salkoff, personal communication; Honore & Lazdunski, Pflugers Arch (1993) 424(2): 113-21).

This source of low-expressing, endogenous BK channels may be an important consideration and caution in the study of low-expressing constructs.

In summary, I did not detect the significant expression of truncated BK constructs and therefore was unable to reproduce the primary finding. I did, however, find an additional source of endogenous BK currents not considered in the original paper. The level of expression from this source is equivalent to the level reported for the truncated constructs.

Having raised the possibility that the observed currents are from endogenous BK channels and providing numbers and observations that support this possibility, other issues are immediately raised. Have the endogenous BK channels been sufficiently characterized? It is not sufficient to compare the currents from truncated-injected oocytes with those from oocytes injected with full-length constructs when considering the possibility of endogenous channel currents. One must make the comparison with

endogenous currents from uninjected oocytes. In the evidence presented in the original work, the currents to which truncated BK currents are compared are in all instances from oocytes injected with a full-length BK construct. There is one reference to study of the TEA sensitivity of endogenous BK currents from *Xenopus* (Krause, Foster & Reinhart, Neuropharmacology (1996) 35(7): 1017-1022), but the data are not shown. To my knowledge a thorough study of the relevant properties of endogenous BK channels in *Xenopus* has not been published.

Resolution of these issues will require either a significant increase in the expression of truncated BK constructs to alleviate any doubt as to the source of the currents being studied, or a thorough study of endogenous BK channels from *Xenopus* to allow for an absolute distinction between the potential sources of current. In the meantime, I find the evidence inconclusive for describing the properties of truncated BK and thus find the interpretation that the C-terminus is not necessary for Ca^{2+} activation premature.

Methods

Each patch was probed as cell-attached and excised in 1-3μM Calcium from -200mV to +200mV (40mV steps) as an initial survey of all observable currents. Pipette resistance ranged from 0.9 2.0 MΩ. Under such conditions BK currents would appear as large openings increasing in frequency and duration over the range of +80 to +200 mV, with a P_o greater than 0.5 at +200mV. Patches containing BK-like currents were then tested over a range of [Ca] and voltages.